# Formation and Characterization of Silica Reinforced Polyvinyl alcohol

A THESIS
SUBMITTED TO THE FACULTY OF THE GRADUATE SCHOOL
OF THE UNIVERSITY OF MINNESOTA
BY

Sunayana Chaudhry

IN PARTIAL FULFILLMENT OF THE REQUIREMENTS
FOR THE DEGREE OF
MASTER OF SCIENCE

Prof. Mrinal Bhattacharya

September, 2011

## Acknowledgements

I am grateful to my advisor Professor Mrinal Bhattacharya for his valuable guidance, encouragement and diligent criticism throughout the execution of this thesis. I would also like to thank him for providing me financial support during the course of my stay here.

I would like to thank Professor Jonathan Chaplin and Professor William T. Tze for serving in my examining committee and analyzing my thesis critically.

I would like to express my sincere thanks to Dr. John Nelson who helped me understand the basics of nanoindentation and scanning electron microscopy. His valuable comments helped me analyze my results better.

I am also thankful to Dr. David Giles who helped me understand the mechanics of Rheometric solid analyzer.

I would like to thank my friends Annu, Sourabh and Sudhir for their support and constant encouragement. In the end I would like to express my deep gratitude to my parents back in India for their unconditional love and support. This thesis is dedicated to them.

# Abstract

This work discusses the construction and characterization of films of polyvinyl alcohol cross-linked with silica nanoparticles that can be used as a potential bone graft for reinforcing the bones weakened with age. Nanocomposites were prepared by adding silica dispersion (10 wt. %) to the solution of polyvinyl alcohol (10 wt. %) in varying concentrations to obtain solution with 39, 60, 78.4 and 120 (wt. %) silica. These solutions were then drawn into thin films (a few nanometres) using a drawbar coater.

The nanocomposites thus formed were characterized using nanoindentation, tensile tests, x-ray diffraction, scanning electron microscopy and infrared spectroscopy . The tensile modulus of the nanocomposite film was calculated to be 8GPa with ultimate tensile strength of 30MPa. The films showed effective cross-linking of the silica with polymer matrix which was studied by scanning electron microscopy, x -ray diffraction and infrared spectroscopy.

To mimic the structure of bone, pellet like crystals of calcium hydroxyapatite were grown on the surface of the surface of the nanocomposite films which further increased the modulus to 11GPa and the ultimate tensile strength to 65MPa. Although the increasing concentration of the silica led to an increase in the modulus of the films, the strength of films decreased thus making them brittlethem brittle.

# Table of Contents

**Page**

# Table of Contents

# List of Tables

**Page**

# List of Figures

**Page**

# List of Figures

**Page**

# List of Figures

**Page**

# Introduction

The structure of human bone is complex, and can be divided into the living and the non-living tissue. The living tissue of the bone is composed of the cells: osteoblasts, osteocytes and osteoclasts while the non-living region comprises the crystalline hydroxyapatite crystals and the collagen fibres. Osteoblasts are the bone forming cells, [Rodan and Martin 1981] osteocytes are the matured osteoblasts that fetch minerals from the blood and deposit them in the formation of apatite crystals while osteoclasts chew the bone [Martin and Sims 2005]. Therefore, the bone formation occurs when the osteoclasts activity is less than that of the osteoblasts.

As shown in Figure 1 the central portion of bone is spongy that has a honey comb structure. Bone cells reside in the lacunae and exchange nutrients with the surrounding fluid by the bone capillaries. The compact bone is the stronger region of the bone made up of the haversian system, which is surrounded with the concentric collagen fibrils and mineral deposits and has the lymphatic vessels running through them [Rho et al. 1998]. The fatigue strength and toughness of bone decrease with age [Martin 1993]. Collagen is the primary toughening mechanism of the bone and has a greater effect on bone toughness, than on strength or stiffness. Changes in collagen structure cause a significant decrease in the toughness of bone [Chatterji and Jeffery 1968].

With age, there is a decrease in the collagen content, which is due to an increased tissue mineralization and decrease in pyrrole cross-links, thus causing osteoporosis. The inter fibrillar pyrrole cross-links in collagen have a much greater influence on the strength of bone than the intrafibrillar pyridinoline cross-links [Wang et al. 2002]. Osteoporosis occurs when there is an imbalance between the new bone formation and old bone resorption [Teitelbaum 2000]. The body may fail to form enough new bone,

or the old bone may be reabsorbed, or both. There is a decrease in the collagen cross-links without an alteration in collagen concentration, and this causes bone to become fragile [Burr 2002].

Thus this weakening of bone with age leading to subsequent fractures can be prevented by reinforcing the bone with material whose elastic modulus and strength are similar to that of bone. A prerequisite for any synthetic material implanted in the body is that it should be biocompatible and not produce an inflammatory reaction. Also, the implanted material should be able to withstand any physiological loading without substantial dimensional change, fracture, or stress corrosion [Christenson 2007]. These have been the two major factors underlying the selection of the materials currently used for orthopedic prostheses.

The starting point for the development of an analogous implant material is the mechanical behavior of cortical bone itself. The stiffness of cortical bone varies between 7-25GPa and the ultimate tensile strength is in the range of 50-60MPa with a small but significant viscoelastic component [Wall et al. 1979]. A balance between modulus and strength is required if the properties of bone are to be matched. A mismatch between the modulus and strength of bone leads to the failure of implant [Ikada 2006].

Therefore the primary reason for the failure of the implant is the occurrence of debonding due to shear loading between fibres and matrix. The loosening of an implant occurs due to the stress shielding of cortical bone produced by an appreciably stiffer implant [Currey 1984]. In short fibres nanocomposite, the fibre ends may increase the stress in the matrix thus increasing the risk of breaking the composite material. The materials used for the reinforcement include the Ti-alloy with high elastic modulus. However, studies have shown that the wear rate in fretting and sliding abrasive tests at the implant/bone interface was high [Bonfield 1998].

CF (Carbon fibre)/PSU (Poly styrene urethane) composite reported ultimate strength to be higher than that of metals used for orthopedic implants, but the elastic modulus was 65% of that of titanium alloy and 30% of that of cast CoCrMo (Cobalt Chromium Molybdenum) alloy. In the 1980s, carbon fibre reinforced ultra-high molecular weight polyethylene (UHMWPE) was also investigated as a bearing surface in joint replacements. This was less successful as the carbon stiffened the UHMWPE, raising the contact stresses and leading to delamination of the CF/UHMWPE interfaces and making resultant black debris a matter of concern [Gasser 2000].

None of the synthetic materials utilized currently parallels the elastic modulus of cortical bone; therefore there is a need to develop a nanocomposite that ensures stress transfer across a tissue-prosthesis interface. From this standpoint, it seems desirable to fabricate a new implant which in addition to having adequate biocompatibility and strength is mechanically compatible with cortical bone. The development of silica nanoparticles reinforced polymer coated with calcium hydroxyapatite as a potential implant material, with mechanical properties analogous to those of cortical bone is discussed in this work.

The silica-polyvinyl alcohol nanocomposite seeks to achieve biocompatibility as well as analogous modulus and strength requirements. Polyvinyl alcohol is water-soluble, biodegradable, biocompatible, gas-barrier, and has high mechanical properties; E=300 MPa (10wt. %), and it is an attractive solution for preparation of PVA-based nanocomposite [Costa et al. 2007]. Silica nanoparticles are water soluble, biocompatible and have a tensile modulus of 198GPa [Wang et al. 2005]. Using them as filler for the construction of the scaffold was believed to increase the modulus and strength of scaffold many folds [Bourlinos et al. 2007]. A theoretical estimate of the modulus was made by using the Halpin Tsai equation as shown in appendix 1.

## Objectives of this Work

The objectives of this work were to construct polyvinyl alcohol scaffold reinforced with silica nanoparticles such that:

(i) The nanoparticles were cross-linked to the polymer and homogeneously distributed throughout the polymer matrix with no phase separation.

(ii) The nanocomposite was coated with calcium hydroxyapatite to mimic the mineral structure and composition of bone.

(iii) The mechanical properties of the scaffold were similar to that of human bone.

# Literature Review

Fabrication of a nanocomposite with improved mechanical properties has been studied with variety of fillers using various techniques. There has been considerable improvement in this area and nanocomposites with improved elastic modulus and tensile strength have been obtained. The various issues in the fabrication of nanocomposites are the phase segregation between the filler and matrix, techniques for dispersion of filler into the matrix and attaining the desired elastic modulus and strength.

Polymers are widely used in bone grafting owing to their biocompatibility, design flexibility, functional groups availability, surface modifiability, light weight, and ductile nature [Hollinger et al. 1996]. Although they have many desirable characteristics, they exhibit low stiffness [Murugan and Ramakrishna 2005]. Therefore the reinforcement of polymers with inorganic fillers having high modulus and strength is desirable. The various nanocomposites developed for the reinforcement of bone are summarized in Table 1.

The elastic modulus and the tensile strength of the nanocomposites developed for the regeneration of bone does not match the properties of bone (Table 1). As can be seen the highest modulus for the majority of nanocomposites cited is lower than that compared to human bone. Hence there is a need for the construction of nanocomposites with enhanced modulus and strength. This section will focus on the preparation of nanocomposites reinforced with modified carbon nanotubes, clay nanoparticles and silica nanoparticles as fillers for the construction of nanocomposites with enhanced modulus and strength. These fillers have high mechanical properties and are modified to have better linkage with the polymer matrix as discussed in the following section.

## Phase Segregation

The successful construction of a nanocomposite is based on the effective load transfer between the organic and the inorganic component. Therefore the filler used in the nanocomposite should be cross-linked to the organic matrix and be distributed homogeneously throughout the polymer matrix. This section will focus on the modifications of the three filler components namely, carbon nanotubes, clay particles and silica nanoparticles and their effect on the enhanced cross-linking with the polymer matrix.

### Carbon Nanotubes (Cnt) Based Nanocomposites

CNT have outstanding mechanical (E=1TPa) and electrical properties [Nadagouda and Varma 2007]. However, the primary issue of concern with the CNT is their dispersion in the polymer. Modification of CNT by a) thermal b) chemical c) substitution techniques [Balasubramanian and Burghard 2005] leads to their improved solubility and hence more applications.

Rouse and Lillehei (2003) introduced carboxyl groups onto the CNT by esterification reactions which were then used for the fabrication of nanocomposites with polyelectrolyte by Layer by Layer technique. Polydiallyldimethylammonium chloride (PDDA) layer was coated onto a silicon wafer followed by the deposition of modified carbon nanotubes. Thus polyelectrolyte nanocomposite was formed.

Mitchell et al. (2002) prepared polystyrene nanocomposites with functionalized single-walled carbon nanotubes (SWCNTs), by the in-situ generation and reaction of organic diazonium compounds. These nanocomposites were characterized using dynamic viscoelastic measurements and contrasted to the properties of polystyrene composites prepared with unfunctionalized SWCNTs at similar loadings. The functionalized nano-composites formed a percolated SWCNT network structure at concentrations of 1 vol. % SWCNT, while the unfunctionalized SWCNT-based composites exhibited viscoelastic behavior comparable to that of the unfilled polymer at twice the loading of SWCNT. This formation of the SWCNT network structure for the functionalized SWCNT-based

composites is due to the improved compatibility between the SWCNTs and the polymer matrix and hence better dispersion of the SWCNT.

Lin et al. (2003) prepared composites with polyvinylalcohol (PVA) and functionalized single-walled and multiple-walled carbon nanotubes. The nanotubes were functionalized in carbodi-imide-activated esterification reactions. PVA and the PVA functionalized carbon nanotubes samples were soluble in highly polar solvents such as DMSO and water. The like solubilites allowed the mixing of the PVA- functionalized nanotubes with the PVA polymer for the wet-casting of nanocomposite thin films. The PVA-carbon nanotubes composite films thus obtained were of high optical quality, without any observable phase separation, and the carbon nanotubes in the films were well-dispersed as in solution. This technique of the functionalization of carbon nanotubes by the matrix polymer is an effective way for the homogeneous nanotube dispersion for obtaining high-quality polymeric carbon nanocomposite materials.

Gojny et al. (2003) modified multi-walled carbon nanotubes (MWCNTs), produced by arc-discharge method, by treating them with oxidizing inorganic acids. The surface oxidation of the nanotubes (o-MWCNTs) was achieved by refluxing the tubes with multi-functional amines. These functionalized nanotubes were embedded in the epoxy resin and the resulting composite was investigated by transmission-electron microscopy (TEM). The functionalization led to a reduced agglomeration and improved interaction between the nanotubes and the epoxy resin.

Zhang et al. (2003) dispersed the SWCNT in 1wt% sodium dodecyl sulphate (SDS) solution followed by ultrasonication, homogenization and centrifugation. To this solution was then added polyvinylpyrrolidone. This modification of nanotubes by addition of SDS led to an increase in their concentration in the nanocomposite from 1wt% to 5wt%.

Geng et al. (2002) chemically modified the carbon nanotubes by fluorination. Modified carbon nanotubes had increased solubility in selected solvents which led to their effective inter-facial cross-linking with polyethylene oxide (PEO). For the

fluorination reaction, 10-15mg purified SWCNTs were dispersed in dimethylformamide (DMF) by sonication. Filtering the solution through a Nylon filter membrane (Milipore, pore size 0.45μm) resulted in a black film on the surface. The film was then peeled off and baked in air at 100°C for several hours. The nanocomposite thus formed had 4wt% CNT distributed throughout the polymer matrix with effective load transfer between the polymer and the nanotubes.

**Clay Based Nanocomposites**

Clay refers to a class of materials made up of layered silicates, among which montmorillonite (MMT) is the most commonly used clay in the synthesis of nanocomposites [Yang et al. 1998]. Clay nanoparticles have a modulus of 178GPa [Fornes and Paul 2003] and are studied as a filler for the polymer nanocomposite.

However, one of the drawbacks of clays is the incompatibility between hydrophilic clay and hydrophobic polymer, which often causes agglomeration of clay mineral in the polymer matrix [Zeng et al. 2005]. Therefore, surface modification of clay minerals is the most important step to achieve polymer nanocomposites [Agag et al. 2001]. Organic treatment of the clay makes it hydrophobic and hence compatible with polymers. Such modified clays are commonly referred to as organoclays.

Chen et al. (2000) synthesized novel segmented polyurethane (PU)/clay nanocomposite. Twelve aminolauric acid (12COOH) and benzidine (BZD) were used as swelling agents to treat sodium-montmorillonite and for forming organoclay (12COOH-mont and BZD-mont) through ion exchange. The silicate layers of organoclay were completely exfoliated in PU in the cases of 1, 3 and 5% 12COOH-mont/PU and in the cases of 1 and 3% BZD-mont/PU nanocomposites as confirmed by X-ray diffraction pattern and transmission electron microscopy studies. A two-fold increase in the tensilestrength and a three-fold increase in the elongation were found for 1% BZD-mont/PU as compared to that of pure PU.

Liu et al. (1997) prepared polypropylene (PP)/clay nanocomposites (PPCN) via grafting-melt compounding by using a new kind of co-intercalation organophilic clay which had a larger interlayer spacing than the ordinarily organophilic clay only modified by alkyl ammonium. One of the co-intercalation monomers was unsaturated so it could tether on the PP backbone by virtue of a grafting reaction. The larger interlayer spacing and strong interaction caused by grafting improved the dispersion effect of silicate layers in the PP matrix, which was confirmed by X-ray diffraction (XRD) and transmission electron microscopy (TEM). The clay loading increased from 0-7 wt% and therefore showed an improvement in the mechanical properties of PPCN. The incorporation of silicate layers also gave rise to a considerable increase of the storage modulus from 0.80 GPa to 1.15GPa demonstrating the reinforcing effect of clay on the PP matrix.

Garcia-Lopez et al. (2003) prepared polypropylene–clay nanocomposites using two different coupling agents, diethyl maleate (DEM) and maleic anhydride. Two different clays, a commercial montmorillonite and a sodium bentonite purified and modified with octadecylammonium ions were used. Functionalization of PP with DEM was obtained in two stages; first PP and DEM were mixed, feeding the compatibilizer dissolved in acetone through a side feeder, by means of a peristaltic pump. In a second stage, acetone solution was added as a catalyzer in order to initiate the grafting reaction. The obtained material was washed with acetone to extract the unreacted functionalizing agent. The relative influence of each factor, matrix and clay modification was observed from structural analysis (SAXS, TEM) and mechanical properties.

**Silica Nanoparticles Based Nanocomposites**

Silica nanoparticles are hydrophilic and hence have to be modified for forming composites with hydrophobic polymers.

Yang et al. (1998) prepared polyamide 6 (PA 6)/silica nanocomposite through in situ polymerization, by first suspending silica particles in caproamide under stirring and then polymerizing this mixture at high temperature under a nitrogen atmosphere. The

silica was premodified with aminobutyric acid prior to the polymerization. The effects of the addition of unmodified and modified silica on the dispersion, interfacial adhesion, isothermal crystallization, and mechanical properties of PA 6 nanocomposites were investigated by using scanning electron microscopy, dynamic mechanical analysis, and mechanical tests, respectively. The results showed that silica was dispersed homogeneously in the PA 6 matrix. The mechanical properties such as impact strength, tensile strength, and elongation at break of the PA 6/modified silica nanocomposites showed a tendency to increase and then decrease with increase of the silica content with a maximum values at 5% silica content, whereas those of the PA 6/unmodified silica system decreased gradually.

Yang and Nelson (2004) prepared polymethylmethacrylate (PMMA)/silica nanocomposites by solution polymerizations which were characterized for their thermal and mechanical properties. IR results showed that both (3-acryloxypropyl) methyldimethoxysilane (APMDMOS) and (3-acryloxypropyl) trimethoxysilane (APTMOS) can serve as reagents for the surface modification of silica, while APTMOS performed better than APMDMOS for the modification of the silica surface. Mechanical properties of PMMA/silica nanocomposites prepared by solution blending showed decreased tensile strength and elongation at break, while materials prepared from solution polymerization performed better than PMMA itself.

**Modulus Enhancement**

**Carbon Nanotubes (Cnt) Based Nanocomposites**

Mamedov et al. (2002) successfully mitigated problems of matrix–SWCNT connectivity and severe phase segregation by preparing the SWCNT composite by layer-by-layer assembly. This deposition technique prevented phase segregation of the polymer/SWCNT leading to an effective crosslinking, for as high as 50% by weight SWCNT. The SWCNT/polyelectrolyte assembly were found to be exceptionally strong with a tensile strength, 220±30MPa and modulus of 35GPa approaching that of hard

ceramics. Because of the lightweight nature of SWCNT composites, the prepared free-standing membranes can serve as components for a variety of long-lifetime devices.

Dufresne et al. (2002) prepared nanocomposite materials from amorphous poly (styrene-co butylacrylate) latex as the matrix using an aqueous suspension of carbon nanotubes in distilled water with 1 wt. % SDS. After stirring, the preparations were cast and the solvent was evaporated. The morphology of the resulting films was examined by scanning electron microscopy and a good dispersion of the filler was observed, except for the 5 wt% filled sample. The mechanical behavior of the nanocomposite in both the linear and non-linear ranges was analyzed. The mechanical characterization displayed a continuous reinforcing effect of the carbon nanotubes without lowering of the elongation at break up to 3 wt%. The thermal stability of the composites was strongly improved by carbon nanotubes loading.

McNally et al. (2005) developed nanocomposite with polyethylene (PE) and multiwalled carbon nanotubes (MWCNTs) with weight fractions of MWCNT ranging from 0.1 to 10 wt% by melt blending using a mini-twin screw extruder. The morphology and degree of dispersion of the MWCNTs in the PE matrix was investigated using scanning electron microscopy (SEM), transmission electron microscopy (TEM), atomic force microscopy (AFM) and wide-angle X-ray diffraction (WAXD). The yield stress of the nanocomposite increased slightly as the loading of MWCNTs was increased up to 10 wt%. However, both the ultimate tensile strength and the elongation at break decreased. The toughness of PE was greatly reduced and addition of MWCNTs above 0.1 wt% made the samples brittle. At lower temperatures modulus increased by about 60% on addition of 0.5 wt% MWCNT compared to neat PE, but decreased to 15% with 7 wt% addition. The value of modulus for all PE/ MWCNT nanocomposites was higher (1KPa to 0.1 MPa) than that of PE alone at all temperatures of processing.

Wang et al. (2006) studied the dynamic mechanical behavior of poly (methyl methacrylate) (PMMA)/acidified multiwalled carbon nanotube (MWCNT) composites

compatibilized with amine-terminated poly (ethylene oxide) (PEO-NH2). The miscibility between PEO and PMMA improved the interfacial adhesion between polymer matrix and MCWNTs, leading to an increase in the storage modulus values of the composites. The effects of PEO-NH2 on storage modulus showed an increase in the modulus from 2GPa to 3GPa.

**Clay Based Nanocomposites**

Liu et al. (1997) proposed preparation of nylon 6/clay nanocomposites by a melt-intercalation process leading to the formation of exfoliated nanocomposite. The modified clay and nylon 6 were mixed mechanically and extruded using the twin screw extruder.X-ray diffraction, DSC and TEM were used to characterize the nanocomposite and the results showed that the crystal structure and crystallization behavior of the nanocomposites were different from those of nylon 6. Mechanical testing showed that the properties of the nanocomposites were superior to nylon 6 in terms of strength and modulus without sacrificing their impact strength. The tensile modulus increased from 2 GPa to 4.1GPa and the yield strength from 68MPa to 96MPa. The increase occurred rapidly with the clay content in the range of 0–15 wt %, but changed little for clay content higher than 15 wt %. This was due to the strong interaction between the nylon 6 matrix and the clay interface, as revealed by X-ray diffraction, transmission electron microscopy.

Fu and Qutubuddin (2000) modified the surface of montmorillonite (MMT) by cationic exchange with vinylbenzyl dimethyldodecyl ammonium chloride (VDAC) in an aqueous medium. This functonialized MMT was added to the Polystyrene for the preparation of nanocomposite. Polystyrene–clay nanocomposites were prepared by free radical polymerization of styrene containing dispersed organophilic MMT. The exfoliated nanocomposites showed an increase in the modulus from 3GPa to 6GPa on addition of 7.6 wt% MMT.

Ma et al**. (**2001) prepared polypropylene/clay (PP/clay) nanocomposites by intercalative polymerization. The nanostructure of the composites was investigated by wide angle X-ray diffractometry (WAXD) and transmission electron microscopy (TEM). The WAXD patterns of the PP/clay nanocomposites showed that the characteristic diffraction peak of the clay disappeared on addition of PP. The TEM image also showed the exfoliated clay was uniformly dispersed in the PP matrix. The composites exhibited higher storage modulus compared to that of pure PP**.** The PP/MMT1 (2.5 wt %, 4.6 wt %, 8.1 wt %, 10.4wt %) composites were prepared and the modulus increased from 1.5GPa for PP to about 2.5GPa for the maximum amount of clay added.

Agag et al. (2001) developed nanocomposites from polyimide and clay with the aim of finding a method for enhancing particularly the tensile modulus of polyimide films. Polyimide–clay hybrids were prepared by blending of polyamide acid and organically modified-montmorillonite (OMMT). Polyamide acid was prepared from the reaction of 3, 3′, 4, 4′-biphenyltetracarboxylic dianhydride (BPDA) and *p*-phenylenediamine (PDA). Also, polyamide acid from pyromellitic dianhydride (PMDA) and 4, 4′-oxydianiline (ODA) was prepared for comparison. OMMT was prepared by surface treatment of montmorillonite (MMT) with ammonium chloride salt of 12-aminolauric acid. XRD indicated that the OMMT layers were exfoliated and dispersed into the poly (amide acid) and polyimide film. Tensile properties measurements of polyimide–clay hybrids indicated that the addition of 2 wt. % of OMMT increased the tensile modulus of BPDA/PDA polyimide up to 12.1GPa, which was 42% higher than the pristine BPDA/PDA polyimide. Tensile modulus of PMDA/ODA also increased up to 6.2GPa, which was 110% higher than that of the original PMDA/ODA polyimide.

**Silica Nanoparticles Based Nanocomposites**

Van-Zyl et al. (2002) constructed inorganic-polymer composite using nanosize silica filler particles and nylon-6 matrix. The composite when examined with TEM

showed silica particles homogeneously dispersed in the matrix. An appropriate choice of organic solvent and pH cont-rol was used to optimize the process. XRD pattern of the nanocomposite showed the silica phase remained amorphous while the polyamide phase was semi-crystalline. Compared to pure nylon-6, hybrid composite showed an increase in impact toughness, elastic modulus as a function of filler percentage.

Bandyopadhyay et al. (2005) prepared organic–inorganic hybrid nanocomposites with Polyamide-6, 6 (PA66), and silica (SiO2) using sol–gel technique. The inorganic silica was prepared by hydrolysis–condensation of tetraethoxysilane (TEOS) under acid catalysis. Infrared spectroscopy was used to study the structure of modified silica in the PA66 matrix. Wide angle X-ray scattering (WAXS) showed that the crystallinity of PA66 decreased with increasing silica content. Dynamic mechanical analysis (DMA) showed significant increase in storage modulus of the nanocomposites as compared to control sample. An increase in Young's modulus and tensile strength of the hybrid films was also seen with an increase in silica content, suggesting significant reinforcement of the matrix in the presence of nanoparticles. Young's modulus increased from 0.6GPa to 0.8GPa and maximum tensile stress showed an increase from 0.8GPa to 1GPa with an increasing silica concentration from 0-10 wt%.

Wu et al. (2005) prepared polypropylene-based composites by melt blending with nano-silica, which was pre-treated by grafting polymerization for surface modification. Tensile moduli and strengths of the composites were determined as a function of the silica content and the amount of the grafting polymers chemically attached to the nanoparticles. The static and dynamic mechanical behaviour models of the nanocomposites were used to study the interfacial interactions and tensile performance of the composites.

Stronger interfacial interactions existed in the grafted silica-filled polypropylene composites as compared to the composites with untreated silica. The modulus of the nanocomposite increased from 1.4GPa to 1.8GPa on increasing the concentration of

silica grafted with PS. An increase in the percentage grafting for various nanoparticles resulted in an increase of interphase thickness, but the interfacial interactions and the tensile performance of the composites were not improved because the agglomeration structure of the nanoparticles.

**Kevlar Based Nanocomposites**

Kevlar is filler that has a modulus of 1.2GPa [Ribelles et al. 1991] and is used for the preparation of nanocomposites that have high modulus and strength. Kevlar has excellent thermal and thermoxidative stability, as well as exceptional tensile strength and tensile modulus when it is spun into fiber. These properties are attributable to chain stiffness and a high degree of molecular orientation and crystallinity. Chemical modifi cation of kevlar, to improve solubility, has been attempted by adding halogens or other chemical substituents on the phenylene rings [Park et al. 2006].

Takayanagi and Katayose (1983) modified the surface of poly(p-phenylene terephthalamide) (PPTA) fiber to provide the fiber surface with several functional groups such as the n-octadecyl group, carboxymethyl group, and acrylonitrile by the polymer reaction via the metalation reaction in dimethyl sulfoxide. The composite of surface modified PPTA fibres by carboxymethyl groups showed remarkable improvement in the mechanical properties. Modulus increased from 152 MPa to 783 MPa and the ultimate tensile strength showed an increase from 19.7 MPa to 27.1 MPa.

Salehi-Mobarakeh et al. (1996) studied the changes in the nanocomposite properties by chemical modifications of the surface of Kevlar fiber leading to an improved fiber-matrix adhesion. This grafted nylon-Kevlar was characterized by ESCA (electron spectroscopy for chemical analysis), DSC (differential scanning calorimetry), and extraction procedures. An increase in the thickness of transcrystalline layer was observed suggesting better fiber-matrix adhesion. Modulus of the polymer reinforced with Kevlar increased from 2.92 GPa to 4.1 GPa while the strength of the polymer increased from 82.2 MPa to 133MPa. Improvement of the mechanical properties was related to better interfacial interactions due to grafted nylon chains.

Mukherjee et al. (2006) reinforced Polystyrene with modified Kevlar fibres and studied effects of the surface modified Kevlar fiber on the crystalline, thermal, dynamic mechanical properties of the Kevlar fiber reinforced syndoitactic polystyrene (s-PS) composites. Thermo gravimetric analysis (TGA) showed significantly improved thermal stability of the modified kevlar fiber composites. Dynamic mechanical analysis showed that an increase in the storage modulus was more pronounced in case of surface modified Kevlar fibers. This was because of the increased fiber/matrix interaction in case of modified Kevlar fiber/s-PS. The modulus of oxy-fluorinated Kevlar fiber nanocomposite increased from 8GPa to 10GPa.

It can be concluded from the discussion above that for most of the nanocomposites, modulus and the strength are much lower than that of cortical bone. Therefore none of the work discussed above provides us with a nanocomposite having properties similar to that of human bone. The nanocomposite constructed by Mamedov et al. , Agag et al. and Mukherjee et al. are an exception. Also, along with having the desirable mechanical properties the nanocomposite should be biocompatible, bioactive and biodegradable so that it can be successfully implanted in the body.

Nanocomposites of PEO and PMMA show a maximum modulus of 3 GPa as discussed above, however they cannot be used as bone implants since these polymers are not biodegradable and therefore will not be removed from body. Also, since the majority of nanocomposites are developed using hydrophobic polymers, their removal from the body after the restoration of bone requires specific conditions such as a change in pH and can lead to the formation of intermediate degradation.

Another issue to be noted is that the even though the modification of filler particles by attaching functional groups, grafting polymers or by cation exchange reactions leads to effective cross-linking of the polymer and the nanoparticles, the extent of cross-linking is limited by the number of functional groups present onto the modified filler. Thus

taking into account the issues of biocompatibility, biodegradation and high mechanical properties we opted to use silica nanoparticles and polyvinyl alcohol. Both of them are water soluble and form effective cross-linkage on being mixed together.

# Materials And Methods

## Materials

Silica nanoparticles (80nm diameter) were purchased from Nanoamor Houston, TX USA, polyvinyl alcohol (99.8% hydrolysed) was purchased from J.T.Baker Phillipsburg NJ U.S.A., polyallylamine (PAH) and trishydroxymethyl amino methane were obtained from Sigma Aldrich, USA. Sodium chloride, sodium bicarbonate, potassium chloride, disodium hydrogen phosphate dihydrate, magnesium chloride hexa-hydrate, calcium chloride dihydrate, sodium sulphate were acquired from the laboratory ((at the Department).

## Methods

### Polyvinyl Alcohol Solution

Polyvinyl alcohol dispersion 10 wt. % was prepared by mixing the PVA powder in 100ml distilled water (DW) and heated to 70 º Celsius(C). The mixture was continuously stirred for 2 hrs until a clear solution was obtained.

Silica dispersion was prepared by adding 10 gm of silica nanoparticles (in small amounts) and 0.5 gm Polyallylamine (PAH) in 100ml of deionised water under gentle stirring. The amount of PAH in the solution was kept low to prevent the aggregation of PAH [Park et al. 2008] chains into clusters thus ensuring the modification of silica by PAH chains.

Due to the large amount of silica present in the solution, silica particles aggregate and hence not all the particles are exposed to the solvent and to the PAH chains present in the solution. All the silica particles that are exposed to the solvent are assumed to be modified based on the fact that a single chain of PAH has a radius of gyration of 2um [Patwardhan 2003] which is much more than the size of a single silica nanoparticle (80nm) [Peng et. al 2005]. Thus, a single chain of PAH wraps around more than one

silica nanoparticle leading to electrostatic interactions between the positively charged amino groups of the PAH and negatively charged hydroxyl groups of the silica. This surface modified silica when added to PVA leads to effective hydrogen bonding between them [Peng et. al 2005].

The surface modified silica-PAH mixture was ultrasonicated at 45 KHz for 1.5 hrs at 25º Celsius (C). A white milky solution was obtained which had silica nanoparticles uniformly dispersed throughout the solution. The effect of of ultrasonication is evident by the SEM image (Figure 29) of the silica nanocomposite (120 wt. %). The size of silica nanoparticles is about 1.5-2 times the original size of the silica nanoparticles, suggesting that the particles did not aggregate much even at such high concentration of silica.

**Simulating Body Fluid (SBF)**

The nucleation of apatite crystals similar to that of human bone requires the deposition of calcium and phosphate onto the polymer surface followed by their growth in conditions similar to that of body fluid. Simulating body fluid had composition similar to that of the body fluid and a pH of 7.4. The composition of SBF is given in Table 2.

The reagents were dissolved in 700ml of water in the order given in Table 2. Before adding the sixth reagent 15ml of hydrochloric acid was added to adjust the pH of the solution to 7.4. A total of 40 ml of hydrochloric acid (HCl) was added. The final volume of the solution was made increased to 1L [Tas 2000].

Calcium nitrate ($Ca(NO_3)_2.4H_2O$ (99%)) and ammonium phosphate $(NH_4)_2HPO_4$ (99%) were used as source of calcium and phosphate phosphate. $Ca(NO_3)_2.4H_2O$ and $(NH_4)_2HPO_4$, 23.56gm and 5.154gm were dissolved separately in 50 ml of SBF individually. $(NH_4)2HPO_4$ solution (pH=11.0) was then added slowly to the solution of Ca $(NO_3)_2).4H_2O$ (pH=11.0) and the volume of final solution was made up to 250ml by the addition of SBF [Tas 2000]. In order to grow the apatite crystals crystalsonto , the surface of the film was negatively charged by placing it in oxygen asher (RF power 100W at a etch rate of 1.34 Å) for 1min. This film was then dipped in the solution above for 5 days and checked for the presence of apatite crystals by SEM.

**Nanocomposite Formation**

Silica dispersion was added in varying concentration to PVA solution (10 wt. %, g PVOH/ml solution) and stirred until a homogeneous mixture containing silica at 39, 60, 78.4 and 120 wt. % (g silica/g PVOH) was obtained. Molecular chains of PVA are attracted to the surface of the silica nanoparticles through hydrogen-bonding interactions between the hydroxyl groups of PVA and Silica and the amide groups of PAH [Peng et al. 2005]. This solution was drawn into thin sheets using a drawbar coater on the glass sheet (Figure 2). It was then left to solidify and after 24hrs (at room temperature) thin polymer sheets of polyvinyl alcohol reinforced with silica nanoparticles were obtained (Figure3).

**Rheometric Solid Analyzer (RSA)**

The RSA was used to measure the bulk modulus and the ultimate tensile strength of the polymer nanocomposite by dynamic frequency sweep test and dynamics strain sweep test. Maintaining the same sample size and thickness of the nanocomposite was necessary to obtain reproducibility of the results. Keeping in mind the brittle nature of the nanocomposite films (at high silica concentration) it had to be ensured that there were no cracks in the sample at the time of loading them onto the rheometric solid analyzer. The presence of crack in the sample could have led to sample failure by causing stress concentration and thus prevent necking at the centre of the sample as desired.

Rectangular specimen approximately 23mm in length, 5mm wide and 0.04mm thick was placed in the sample holder. The thickness of the film was measured using the micro calliper and averaged over the entire length of the sample.

For measuring the modulus of the sample, the following factors had to be taken care of. At the time of loading the sample onto the sample holder the pre-tension was set to zero and the strain was set on the order of $10^{-3}$. The test was conducted at room temperature (25 $^{o}$C). The RSA used in this experiment had a gauge length of 22.4mm and therefore the minimum length of the film that could be mounted onto the RSA had to be 35mm in length since the films were clamped at either end to provide a firm grip. On

mounting the first end of the film onto the specimen holder the pretension was set to zero followed by gripping the other end. The stress-strain curve for the specimen was obtained under similar conditions as for the modulus measurement at a strain rate of $10^{-3}$ mm/min.

**Nanoindentation**

MTS Nanoindenter-XP (Characterization facility at the University of Minnesota) was used to carry out the nanoindentation of the nanocomposite film. The standard hardness and elastic modulus test was conducted on the polymer sample and the sample stiffness, modulus and loading and unloading curve was obtained. The nanocomposite film was cut 1cm*1cm in size and was glued to the aluminium stub which was then placed onto the sample tray.

Berkvoich indenter (Characterization facility at the University of Minnesota) was used to indent the polymer surface. The indenter was calibrated by running five indents on fuse quartz to check for the alignment of the tip with the surface. The accuracy of the results given by the nano-indenter was measured by calculating the modulus of a known material, fused quartz was used in this case that had a modulus of 74 GPa. A minimum of ten indents were run per sample to check for the reproducibility of results.

**Scanning Electron Microscopy (SEM)**

JEOL 6500 SEM (Characterization facility at the University of Minnesota) was used to study the morphology of the polymer nanocomposite on addition of silica nanoparticles and on coating with calcium hydroxyapatite. The films did not require any coating for SEM. The polymer film was cut to 1cm*1cm in size and was placed on the sample holder using the carbon tape. The sample was placed in vacuum at a pressure of $10^{-2}$ Pa. Samples were analyzed at magnification ranging from 500X to 100,000X.

**Attenuated Total Reflectance Spectroscopy (ATR)**

Nicolet Series II Magna-IR System 750 FTIR (Characterization facility at the University of Minnesota) was used to study the chemical bonding of the PVA-silica and also the hydroxyapatite coating on the nanocomposite. The polymer film was cut to 1cm*1cm in size and was placed on the sample holder and the contact between the sample and glass prism was guaranteed by covering the sample with a lid.

**X-Ray Diffraction (XRD)**

Changes in the crystalline structure of polyvinyl alcohol after the addition of silica nanoparticles were studied by XRD patterns. This technique was also used to study the effect of increasing silica concentration on the original PVA crystal structure. BRUKER D8-advance X-ray diffraction meter (Characterization facility at the University of Minnesota) with Cu, Kr radiation (0.154 nm) was employed to carry out wide angle X-ray diffraction (WAXD) test of nanocomposites.

Polymer films were cut to 1cm*1cm in size and were placed in square shaped sample holder. Before conducting the actual test, the equipment was calibrated by running a test for corundum and comparing the result with the standard chart. A scanning rate of 0.2°/min and diffraction angle from 5° to 90° were taken. Bragg's equation, $N\lambda = 2d\sin\theta$, was used to calculate the crystallographic spacing.

## Fundamentals Of Mechanical And Chemical Characterization

### Modulus of Nanocomposite

The DMA is based on applying sinusoidal stress to the nanocomposite at a controlled strain rate. The sinusoidal stress varies with the frequency and at high stresses the bonds between the polymer matrix and the filler will be stretched and can break if the interactions are weak. However, if the polymer is bonded firmly to the filler the bonds remain steady and some bonds may break if the stress is applied for long period of time. This effect is called polymer damping; some bonds may break while some new bonds may appear between the filler particles or the matrix.

Thus, polymers that are strongly bonded to the fillers show a linear plot for the storage modulus versus the frequency. As the time of application of stress increased some bonds between the polymer and the filler start breaking and therefore the modulus deviates from the typical linear behavior [Colo et al. 2004]. This damping effect can be seen in the plot of modulus versus the frequency.

The modulus of a composite is the combined moduluscombined modulus of the matrix and the fibers. There can be various shapes of fibers with different orientations in the polymer matrix which affects the modulus of the nanocomposite. The theoretical calculation for spherical nanoparticles randomly distributed throughout the matrix is given by Halpin Tsai equation [Hsueh 2000]:

**Equation** 1
$$\frac{E_o}{E_m} = \frac{1 + \varepsilon\eta f}{1 - \eta f}$$

**Equation** 2
$$\eta = \frac{\frac{E_f}{E_m} - 1}{\frac{E_f}{E_m} + \varepsilon}$$

$E_o$ – Modulus of the nanocomposite obtained

$E_m$– Modulus of polyvinyl Alcohol (0.3GPa)

$E_f$ – Modulus of silica nanoparticles (198GPa)

$\eta$ – Clumping factor =2 for spherical particles.

$f$ – Volume fraction of silica nanoparticles in the composite.

$\varepsilon$ – $2+ 40\ f^{10}$

The Halpin Tsai equation was used to compute the modulus of composites with random butrandom but homogeneous particle distribution [Kim et al. 2006]. The test specimen was about 23mm in length, 5mm wide and .05mm thick. A 10g force was applied to the specimen until there appears necking a visual necking at the centre of the sample. Data points were collected for the storage and loss modulus.

**Stress-Strain Curve**

The ultimate tensile strength (UTS) of the nanocomposite was determined by loading the rectangular sample material uniaxially in tension. The force applied to the material pulls the polymer cross-linked to the filler such that the bonds between them stretch and if the force applied increases the critical limit of the elongation the material might deform permanently. The stress –strain curve obtained on applying this force to the help us determine the strength and the toughness of the material. As the area under the curve (stress-strain) increases, the toughness of the material increases.

**Nanoindentation**

Nanoindentation is designed to probe material behavior on the nanoscale. Proximal probe tips such as the scanning force microscope (SFM), were used both to perform the indentations and to investigate mechanical properties of materials by indenting the test material with a diamond tip to depths of 100 to 1000 nano-meters while measuring the force-displacement response [Briscoe et al. 1998]. NanoXP was used to conduct the experiments.

The force acting on the tip is measured as a function of the indentation depth, and this relationship allows mechanical properties, such as stiffness and Young's modulus, to be determined. As the indenter tip penetrates the material the force experienced on the tip

due to the cross-linked silica and polyvinyl alcohol is measured. It is this force per unit area when plotted with the penetration depth gives the loading–unloading curve used to calculate the modulus and the stiffness of the material. Thus, nanoindentation is used as a tool to study the relationship between the microstructure, strength and toughness of materials. The various mechanical properties studied by nanoindentation are [Zeng and Chiu 2001]:

Mean contact pressure = Load applied / Actual area

Hardness = Load applied / Actual area

Modulus = Stress/ Strain

The indenter is generally made from diamond and has an axis symmetric or pyramidal geometry with a small radius of curvature at the apex, since the indenter blunts with continued operation [Bull 2005]:

**Equation** 3 $$h_p = h_{max} - \varepsilon \frac{P_{max}}{S}$$

$h_{max}$ – maximum depth of penetration of the indenter into the surface.

Ɛ – 0.75 for Berkovich indenter [Fischer-Cripps 2006]

$P_{max}$ – maximum load on sample

S – Stiffness of the sample = slope of unloading curve

$h_p$– elastic-plastic contact depth

**Equation** 4 $$A = 24.56 h_p^2$$

A- Area of contact of the indenter (Actual area)

**Equation** 5 $$E^* = \left(\frac{1-\upsilon_s^{\,2}}{E_s} + \frac{1-\upsilon_i^{\,2}}{E_i}\right)^{-1}$$

E*– Reduced modulus of the system.

$E_s$– Modulus of sample

$E_i$– Modulus of indenter (1141GPa)

$V_s$– Poisson ratio of sample (0.3)

$V_i$– Poisson ratio of indenter (0.07)

The modulus of the sample can be calculated from the above equation [Zeng and Chiu 2001]. Hardness of the sample is defined as the load applied per unit area at maximum penetration.

**Equation** 6 $$H(c) = \frac{P_{max}}{c\, h_c^2}$$

The depth beneath the specimen free surface within the circle of contact is given by the case of the unloading data in a nanoindentation test, we consider the contact conditions at this point to be entirely elastic (Figure 4). That is, we can unload and reload as many times without any further plastic deformation taking place.

**Scanning Electron Microscopy (SEM)**

SEM was used to study the topography of the sample under analysis. Samples were viewed at various voltage and magnification on order to get the exact details of the surface under analysis.

**Attenuated Total Reflectance Spectroscopy (ATR)**

When the frequency of incoming infrared radiation on a material matches the frequency of the vibrations of the bonds present in the material, energy is absorbed by these vibrating bonds. This causes stretching of the already stretched bonds. This absorbed energy increases the energy of the individual bonds leading to an increase in the amplitude of the vibrations but does not change the bond frequency. This change in amplitude can be seen as a peak at the frequency at which the energy is absorbed in the IR spectrum. However, for samples that cannot transmit light, this analysis cannot be performed in the usual absorbance mode. This is when the ATR mode of IR spectroscopy can be used.

**X -Ray Diffraction (XRD)**

X-Ray Diffraction Analysis (XRD) was used to study the crystalline structure of the materials, crystallite size and imperfections. When x-ray photons collide with

electrons, some of the photons from the incident beam get deflected away from the original direction of travel. If the wavelength of these scattered x-rays remains the same the process it is referred ascalled elastic scattering, it is only the momentum that gets transferred in this process.

The peaks in x-ray diffraction pattern are directly related to the atomic distances in the crystalline structure. For a given set of lattice planes with an inter-plane distance of d, diffraction is given by [Strawhecker and Manias 2003]:

$$N\lambda = 2d\sin\theta$$

Θ- Angle between the lattice plane and the diffracted beam

λ – Wavelength of the X-Ray beam

N- Integral multiple of wavelength

# Results And Discussion

## Dynamic Modulus

The changes in the bulk modulus and the yield stress with increasing silica concentration in the nanocomposite were studied by performing the dynamic frequency sweep test and dynamic strain sweep test respectively.

When a sinusoidal stress is applied to the material it causes the material to deform and that is measured as strain. The ratio of the sinusoidal stress to strain is defined as complex modulus, that can be divided into storage modulus and the loss modulus. The storage modulus refers to the ability of a material to store energy and is a measure of the elasticity of the material [Colo et al. 2004]. The loss modulus represents the energy dissipated as heat when the sample suffers deformation. This is the viscous portion of the sample.

The change in the bulk modulus with changing silica concentration is demonstrated by plotting the graph of bulk modulus versus frequency (at which the cyclic loads were applied to the polymer nanocomposite film) while the stress-strain curve gives information about the ultimate tensile strength of the film. Taking into account the viscoelastic nature of polymer nanocomposites, the elastic range of the PVA-silica nanocomposite film was determined by strain sweep test (Figure 5) where the bulk modulus was plotted versus the strain. The modulus of the nanocomposite is linear until about $6*10^{-3}$ value of the strain and shows a decrease thereafter followed by a steep decrease at $10^{-2}$ value of strain. The region of the graph in the $10^{-3}$ range of strain is considered to be the elastic and the sharp decline at a strain of $10^{-2}$ represents the plastic range of the nanocomposite. The decrease of the modulus in the elastic region of the nanocomposite can be explained as the beginning of the bond rearrangement in the nanocomposite due to the applied sinusoidal stress. Therefore the elastic range of strain

was chosen as the workable range for performing the dynamic frequency and the strain sweep test.

**Reproducibility of Data**

The reproducibility of the results obtained by dynamic tests stated above was confirmed by performing the test on four films of each type (silica nanoparticles concentration). The tests showed that the results are coherent for a given concentration of silica in nanocomposites.

**Sources of Error**

The possible sources of error for the dynamic testing were the inhomogeneous nature of the polymer films leading to a non-uniform thickness of the film. Another issue of concern was the loading condition at the start of test. The sample should have no pretension since an initial tension in the sample will result in an error in the force being applied to the sample.

The above sources of error were avoided by preparing a homogeneous solution of silica nanoparticles and polyvinyl alcohol by continuous stirring followed by drawing it into films of uniform thickness using a drawbar coater.

In order to avoid the pre-tension on the sample, the reading for tension reading of the film was checked on the instrument after clamping each end of the film between the grips. Any load recorded after clamping the first end of the film was set to zero using the calliper provided on the RSA. Tension (load) recorded after clamping the second end of the film between the grips was also set to zero using the calliper. The difference between the two readings of the calliper was calculated as the strain offset of the sample and was added to give the final length of the sample.

The bulk modulus of the nanocomposite increased with increasing silica concentration as shown in Figures 6, 7, 8 and 9. As the concentration of silica increases from 39 wt. % to 120 wt. % the modulus of the nanocomposite increases due to increased crosslinking with the filler particles. Nanocomposite (silica concentration 120 wt. %) coated with apatite shows a further increase in modulus as shown in Figure 10.

The young's modulus as a function of silica loading is shown in Figure 11. The increase in modulus as explained earlier is due to the enhanced cross-linking between the silica (E=198 GPa) and PVA. The Young's modulus of PVA film (10 wt. %) was measured as 0.3GPa. In cross-linked polymer systems, the modulus increases linearly with the filler volume fraction [Manias et al. 2001] whereas for silica nanoparticles much lower filler concentrations increased the modulus sharply and to a much larger extent. This can be inferred by dramatic enhancement of the modulus of the PVA film (E= 0.3 GPa) on adding small amount of silica dispersion.

The dramatic enhancement of the young's modulus from 0.3GPa to 3GPa for silica filler (39 wt. %) concentrations cannot be attributed to the introduction of silica alone. According to a theoretical approach the polymer matrix gets physio-sorbed onto the surface of silica (as shown in Figure 3) due to the interaction between the negatively charged hydroxyl group and the positively charged amide groups of the PAH and hydrogen bonding between PVA and silica [Bandyopadhyay et al. 2005].

Also, due to the high aspect ratio of the modified silica nanoparticles, the surface area exposed to polymer is large and therefore a dramatic increase in the modulus on addition of silica is observed. The increasing concentration of silica nanoparticles showed an increase in the modulus of the nanocomposite film. The highest modulus is obtained for the nanocomposite with silica concentration of 120wt. %.

The results obtained by RSA are summarized in Table 3 and 4. Modulus of the nanocomposites was calculated theoretically by using the Halpin Tsai equations as shown in appendix 1. A comparison of the theoretical modulus calculated by Halpn Tsai equation shows a slight difference in results obtained experimentally as shown in Table 4. This difference in the result may be explained as follows:

A theoretical calculation for the modulus assumes same strain in the matrix and fibre when the sample is clamped in the sample holder in RSA. However it is very difficult to achieve these conditions in actual settings. Usually only the surface of the sample can be clamped, so the strain is not homogeneous in the entire cross-section. This "skin effect" explains a lower apparent modulus [Ribelles et al. 1991].

The other factor that may cause this mismatch of result is the random distribution of the nanoparticles in the matrix leading to improper strain distribution in the nanocomposite [Ribelles et al. 1991]. Also, the imperfect adhesion of the nanoparticles and the matrix may cause the improper load transfer and hence an error in the modulus.

Coating the surface of nanocomposite with calcium hydroxyapatite further increased the modulus to 11GPa (Figure10) and was an expected result since the modulus of apatite crystals is 117GPa [With et al. 1981]. The nanocomposite (120 wt. % silica concentration) was coated with 0.02± .005mm thick (measured with the micro calliper) apatite layer is expected to show an increase in the modulus as shown in appendix 2. Theoretical calculation predicts the modulus of the nanocomposite coated with apatite as 13 GPa as can be seen in appendix 3. However the experimental results show the modulus of the apatite coated nanocomposite to be 11 GPa. The difference in the result may be explained on the basis of ineffective load transfer between the apatite coating and the polymer resulting in the lower value of the experimental modulus.

From the graphs (Figure 6, 7, 8, 9 and 10) for the modulus of the nanocomposite films it can be seen that the modulus of the films is almost linear in the frequency range of 120Hz to 20 Hz for all the films. However, a decrease in the modulus of the nanocomposite in the frequency ranges of 0-20Hz is seen.

This can be explained as the possible damping effect of the polymer [Colo et al. 2004] and is a typical for the nanocomposites. The application of sinusoidal stress to the polymer causes the material to stretch and thus in the frequency range of 0-20Hz the material shows amorphous behavior due to the rearrangement of the cross-links in the polymer and hence loses its elasticity. Thus, a possible rearrangement of the polyvinyl alcohol cross-linked silica nanoparticles leads to amorphous behavior of the films at lower range of frequency.

It can also be observed that the experimental results show deviation in the modulus amongst the four different samples used for modulus measurement (Figures 6, 7, 8 and

9). This deviation can be explained as the possible drawback of the technique used for casting the nanocomposite films using the drawbar coater. There might be a possible clumping of the silica nanoparticles, their inhomogeneous distribution in certain areas in the polymer due to improper mixing or a minor difference in the cross-linking of nanoparticles with the polymer. Further addition (above 120 wt. %) of the silica dispersion to the PVA solution was limited since the films became brittle and crumpled. This could be attributed to the increase in the surface tension in the film due to large amount of silica nanoparticles [Nuriel et al. 2005].

**Stress-Strain Curve**

A typical nanocomposite is expected to show viscoelastic behavior on application of increasing force. This was observed for the nanocomposite thus fabricated. The ultimate tensile strength of the PVA (10 wt. %) is 3.5MPa. On addition of silica nanoparticles, 39 wt. % to the polymer the ultimate tensile strength of the polymer increases to 6MPa as shown in Figure 12. This showed that the addition of silica nanoparticles increased the strength of the composite film.

On further increasing the amount of silica nanoparticles concentration in the nanocomposite the ultimate tensile strength shows a marked increase to 25MPa (Figure 13). This may be explained on the basis of effective cross-linking (hydrogen bonding) of the silica nanoparticles with other nanoparticles and also with the polymer matrix. The increased hydrogen bonding between the silica and PVA leads to increased stiffness and an increase in the strength of the film. The maximum UTS of 45MPa is seen for the nanocomposite with the silica concentration 78.4 wt. % (Figure 14). On increasing the concentration of silica to 120 wt. % the strength of the composite decreases to 33MPa (Figure 15). This decrease may be due to some unbonded silica nanoparticles in the polymer matrix. As the concentration of silica increases nanoparticles aggregate due to reduced inter-particle distance and therefore some silica nanoparticles are left unbonded to PVA. This aggregation of nanoparticles makes the nanocomposite with 120 wt. %

silica brittle as compared to the lower wt. % silica nanocomposite. Thus, the nanocomposite undergoes ductile to brittle transition on increasing the silica concentration from 78.4 wt. % to 120 wt. % [Bandyopadhyay et al. 2005].

On observing the individual graphs for the strength of the nanocomposite the deviation in the individual results for a given nanocomposite can be seen. This slight difference in the individual results can be explained as earlier due to a possible difference in the arrangement/linkage of the silica nanoparticles in a particular region of the nanocomposite which may be due to the inherent nature of the technique used for the nanocomposite development.

The strength of the nanocomposite however increases on coating with calcium hydroxyapatite (Figure 16). This is an expected result since the apatite crystals deposit onto the surface of the nanocomposite as pellets and thus increase the strength of the nanocomposite. The strength of the nanocomposite with 120 wt. % silica increased from 33MPa to 65MPa on coating with apatite.

**Nanoindentation**

Berkovich indenter was used to indent the surface of the polymer nanocomposite and the stiffness, elastic modulus and the elastic-plastic deformation of the nanocomposite was studied. The Poisson's ratio and maximum depth of penetration of the indenter were predetermined as 0.30 and 2200nm for all samples. The penetration depth of the indenter was determined as about 1/10th of the total thickness of the sample in order to avoid the influence of the properties of the substrate onto which the sample is loaded [Bull 2005]. Therefore, the penetration was optimally determined to extract all the information of the polymer sample and avoiding the influence of the substrate.

**Reproducibility of Data**

The reproducibility of data was confirmed by indenting the surface of the polymer 10 times at different loads and the modulus of the nanocomposite was determined as the intercept at low loads.

**Sources of Error**

Initial penetration or zero point determination is very important procedure in nanoindentation testing. This is important because the contact point determines the datum of the displacement measurement. This was taken care of by determining sharp rise in the force data as the indenter hits the surface of the sample. The point of contact was thus taken as the start point for the experiments. Material effects may also cause a significant error in the results obtained by the nanoindentation. Indenting a soft material while placing it on a hard substrate may reflect the properties of the substrate in the final results obtained for the sample hardness and the modulus since the indenter will penetrate the film and calculate the properties of the hard substrate. If the substrate is soft the load applied may bend the substrate and not penetrate the sample enough to study the properties of the material at low load conditions. The above mentioned substrate effects were avoided by using aluminium as the substrate for performing the nanoindentation.

The loading–unloading curve for the hybrid nanocomposite with silica concentrations of 39 wt. %, 60 wt. %, 78.4 wt. %, and 120 wt. % and of nanocomposite coated with calcium hydroxyapatite respectively are shown Figures 17, 18, 19, 20 and 21 respectively. The initial part of the curves till 1900nm is the loading curve or the elastic region of the nanocomposite film, followed by this is the region of constant load for the polymer film to creep and after this is the unloading curve where occurred small degree of plastic deformation. The load on the polymer increases as a function of the penetration depth until the material reaches the yield point. This is defined as the point of maximum load. As the indenter moves into the sample the contact radius also increases and there is a transition from elastic region to plastic region. The contact increases as the indenter penetrates the surface of the film under analysis. The pressure on the system increases in the elastic zone until the transition zone followed by the plastic zone until it level offs to a constant value and this is called the hardness of the sample.

The unloading region of the curve is when the indenter tip moves out of the sample after indenting the surface. Therefore the force on the tip decreases as the tip moves out. For a purely elastic contact of the indenter with the sample surface the loading curve

overlaps with the unloading curve. For an elastic-plastic contact, the unloading curve is different to the loading curve and the area enclosed between them represents the energy lost (as heat) during plastic deformation [Fischer-Cripps 2006]. The slope of the unloading curve at any point is called the contact stiffness.

As discussed earlier addition of silica increases the strength of the nanocomposites, this is demonstrated by the increasing maximum loads applied to the composite films from 13mN to 33mN in Figures 17, 18, 19. The modulus increases with increasing silica concentration. This is due to the increasing crosslinking of the silica particles with the polymer and with other silica particles. The results obtained by the nanoindentation are consistent with that calculated by the RSA i.e. higher modulus with increasing silica concentration. The modulus obtained by this technique is an average of the modulus obtained by applying a varying load on the sample. The method involves making a series of indentations on the surface of the nanocomposite and calculating the force required to reach 2200nm. This force is then used to determine the maximum load the material can withstand. The slope of the load versus the displacement curve is used to calculate the elastic modulus of the nanocomposite. As can be seen in Figure 20 there is a decrease in the value of maximum load to 28mN. This can be explained on the basis of the ductile to brittle transition of the nanocomposite (on increasing the silica concentration from 78.4 wt. % silica to 120 wt. % silica) due to the aggregation of the silica nanoparticles in the polymer matrix.

On coating the surface of nanocomposite with silica concentration of 120 wt. % with calcium hydroxyapatite crystals, (Figure 21) it can be inferred that the strength of the nanocomposite increases as the maxim load applied increases to 40mN. This is expected as apatite increase the strength of bone and hence the results are concomitant with the theoretical data. The slope of the unloading curve gives the stiffness of the sample.

The contact stiffness increases with an increasing penetration of the indenter tip into the sample surface due to increasing in the cross-linking with increasing depth.

Therefore, irrespective of the sample type, the contact stiffness increases as the indenter moves inside the sample. This can be evaluated from the slope of unloading curve.

Nanoindentation technique is also used to measure the modulus of the nanocomposite. However, the modulus thus obtained is the reduced modulus of the system i.e. the combined modulus of the sample and the indenter. The actual modulus of the sample is calculated in appendix 3.

The change in elastic modulus of the nanocomposites with increasing silica concentration is studied (Figures 22, 23, 24 25 and 26). The modulus increases with increasing silica concentration. As discussed before, this is due to the increasing crosslinking of the silica particles with the polymer and with other silica particles. The modulus obtained by this technique is an average of the modulus obtained by when a load is applied to the sample while making the indents on the surface. It is necessary to obtain a sufficient number of data points at low loads so that the data near the lower end of the depth axis captures, as much as possible, the film properties. Once obtained and plotted, the modulus is calculated as the point at which the data points intercept the modulus axis at low loads.

As can be inferred from the loading-unloading curves, a varying load was applied on the nanocomposite and the modulus of the film was obtained. The modulus varied over a certain range for the loads plotted. This variation in modulus is due to the inherent nature of the nanocomposite i.e. the slight difference between the various points of the nanocomposite due to not so homogeneous distribution of the nanoparticles in the nanocomposite. Therefore the modulus of the nanocomposite is estimated by calculating the average of the modulus obtained by each indentation. The modulus of the nanocomposite increased on being coated with apatite as shown in Figure 26.

On comparing the results obtained for the modulus of nanocomposite with the theoretical calculation for nanoindentation (Table 4), a difference is observed in the results. This may be due to the fact that the modulus reported experimentally is an average over the range of the loads used to carry out the indentation. The experimental and theoretical results are summarized in Table 4.

Thus, it can be seen in Table 4 that the mechanical properties of the nanocomposite obtained by RSA and Nanoindentation are comparable and hence can be taken as valid results, since both techniques determine the same modulus based on different principle as discussed before. The result for the modulus and tensile strength for the nanocomposite (with varying silica concentrations) is concomitant amongst the various techniques. This can be explained as follows, though there is a difference between the kinematics of each technique. The RSA as described earlier measures the modulus by applying sinusoidal stress and therefore tries to pull the silica nanoparticles apart from the polymer.

The modulus thus measured by this technique determines the ability of the bonds to stretch on application of sinusoidal stress wave. The tensile strength was measured by loading the rectangular sample uniaxially in tension. The force applied to the material pulls the polymer cross-linked to the filler such that the bonds between them stretch and if the force applied increases the critical limit of the elongation the material might deform permanently.

Both these techniques have different kinematics but they determine the storage modulus i.e. the energy stored inside the material by measuring the bond stretching capacity of the nanocomposite under applied stress the results obtained by both these techniques should be in agreement and this is validated by Table 4.

Nanoindentation measures the force exerted on the tip of the indenter as it penetrates the surface of material. The force acting on the tip increases until the point of maximum load. The increasing force on the indenter tip is due to the enhanced cross-linking of the polymer and the silica nanoparticles. The force acting on the tip estimates energy stored in the nanocomposite [Fischer-Cripps 2006]. The slope of the curve obtained by plotting force with the penetration depth is used to determine the modulus of the material. The energy stored in the bonds was used to calculate the modulus and the strength of the material. The results obtained by all the three techniques give same values as can be seen in Tables 4, 5 and 6.

Loading and unloading curves from nano-indentation provide information about the hardness of the material. Hardness is defined as the resistance of the material to

deformation due to constant load from compression. Hardness is a measure of a material's flow resistance. This is dependent on the local structure of the material at the elastic-plastic transition and during subsequent plastic straining. Based on the above discussion and the results obtained from the theoretical calculation (Table 5) for hardness it can be concluded that the heterogeneity or the surface energy of the nanocomposite increases with increasing silica concentration. This is due to the fact that the presence of bonded and un-bonded particles in the polymer matrix increases the randomness/energy of the composite. Hence there is a resistance to deformation. Bonding amongst the silica nanoparticles in a not so orderly manner causes a disordered arrangement in the nanocomposite and hence a decrease in the hardness with increasing silica concentration.

**Scanning Electron Microscopy (SEM)**

SEM was used to study the morphology of the nanocomposites fabricated and to determine the shape and size of the calcium hydroxyapatite crystals grown on the surface of the polymer nanocomposite. Energy dispersive x-ray analysis (EDX) was also conducted to analyze the chemical composition of calcium hydroxyapatite. The micrographs obtained by Scanning electron microscopy shows a highly cross-linked network of PVA/silica hybrid (Figure 27). Magnification of the nanocomposite (78.4 wt. %) to 10,000X shows an intricate silica-polymer structure, showing a highly cross-linked polymer matrix (Figure 28). As discussed earlier the increasing concentration of silica in the polymer matrix is expected to increase the silica cross-link and hence an increase in the modulus of the nanocomposite. The increased silica concentration also leads to an increase in the sample stiffness; this can be seen from the slope of the unloading curves for the nanocomposites. Since the concentration of silica increases the films become stiffer and hence the maximum load applied on the sample also increases as can be seen in the results for nanoindentation.

The results obtained by RSA, nanoindentation and SEM are thus in accordance with the theoretically expected results. The morphology of the nanocomposite changes with the change in silica concentration as can be seen from the Figures 27 and 28. As was

expected the increasing silica concentration leads to an increased cross-linking between the polymer and the nanocomposite and therefore increase in modulus, stiffness and strength of the films was observed. The changes in morphology such as the enhanced cross-linking between the silica nanoparticles and the polyvinyl alcohol, aggregation of silica nanoparticles corresponding to the increased silica concentration were confirmed by studying the micrographs of nanocomposites at different silica concentration.

On observing individual silica nanoparticles in the polymer nanocomposite it is seen, that the particles aggregate inside the matrix and therefore show an increase in size (on the order of 100nm Figure 29) as compared to the original 80nm particles. Though maximum number of nanoparticles are cross-linked to the PVA matrix some particles get cross-linked with each other than the polymer and the material becomes brittle. This ductile to brittle transition of the nanocomposite thus formed is therefore assumed to be occurring due the addition of large amounts of the silica (120 wt. %) and thus a possible decrease in the inter-particle distance [Peng et al. 2005]. The RSA and the nanoindentation results for the apatite coated nanocomposite show an increase in the modulus due to the expected deposition of the apatite crystals. The presence of these crystals was confirmed by performing the SEM of the nanocomposite coated apatite. As shown in Figure 30, the calcium hydroxyapatite crystals grown on the surface of the nanocomposite can be clearly seen as pellets. The pellet like apatite crystals were on the size range of 10 microns. The chemical composition of apatite crystals showed a Ca/P ratio of 1.67 as confirmed by EDX in Figure 31 [Asada et al. 1998].

Thus, the SEM provided an insight into the morphology of the nanocomposites structure on addition of silica nanoparticles and deposition of hydroxyapatite crystals and thus validated the assumptions made for the explanation of the results for nanoindentation and RSA.

**Attenuated Total Reflectance Spectroscopy (ATR)**

ATR was used to study the chemical cross-linking between the polymer and the nanocomposite. A change in the chemical bonding of various atoms was seen on the

addition of silica nanoparticles. This thus confirmed the effective linkages between the polyvinyl alcohol and nanoparticles.

A comparison of the IR spectra of PVA and PVA-Silica (Figure 33 and 34) shows a broad transmittance around 3200 -3500 $cm^{-1}$ instead of a single peak attributed to the O-H stretching vibrations for the absorbed moisture and hydrogen bonded hydroxyl groups present in the samples [Bandyopadhyay et al. 2005]. Upon the addition of silica nanoparticles, a change in the chemical bonding of various atoms (such as the bonding of silica with backbone of PVA and with hydroxyl groups in water) is observed. The presence of silica in the nanocomposite is evidenced by the broad transmittance around 3200$cm^{-1}$ due the hydroxyl bonds [Jang and Park 2005]. The hydroxyl groups interact not only with PVA but also with other silanol groups (Si-O-Si) formed in the system, or with the hydroxyl groups in water.

A strong transmittance (Figure 33) due to C-O symmetric stretch appears at 920 $cm^{-1}$ in PVA due to etherification reactions in some vicinal O-H groups present in PVA leading to the formation of aliphatic ester ($CH_3CH_2$-O-$CH_2CH_3$) during its dissolution in boiling water. In PVA-Silica this peak area is increased and the peak is shifted to1000 $cm^{-1}$ due to the influence of Si-O stretching vibration of silanol. Broadening and shifting of the peak transmittance area is possibly due to extensive hydrogen bonding between silanol and PVA [Bandyopadhyay et al. 2005].

This confirms the formation of extensive hydrogen bonding between silica and PVA. Transmittance due to O-H in-plane deformation vibrations is seen around 1300 $cm^{-1}$ which overlaps with the C-H deformation vibrations in the same region and hence cannot be separated.

Strong transmittance observed at 900 $cm^{-1}$ in pure PVA is due to the C-O stretching and O-H bending vibrations [Bandyopadhyay et al. 2005]. These vibrations overlap with the Si-O-Si vibrations. With increasing concentration of silica this peak shifts towards higher side, other transmittance bands such as the asymmetric Si-O-C stretch (due to chemical cross-linking of silanol and PVA) and asymmetric C-O stretch can also interfere in this region.

A strong transmittance band of almost equal intensity is noticed for all the samples in the region of 800 $cm^{-1}$ due to out-of-plane O-H deformations [Bandyopadhyay et al. 2005]. Therefore, PVA-silica appears to form an interactive organic-inorganic hybrid system, where the inorganic silica phase is hydrogen bonded to the organic phase of poly vinyl alcohol.

The bands for PVA-silica composite coated with apatite (Fig 34) at 962.6 and 1040 $cm^{-1}$ are the fundamental frequencies of the phosphate ion groups. The bands at 3571-3572 $cm^{-1}$ and at 631-632 $cm^{-1}$ derived from stretching mode of OH groups in $Ca_{10}(PO_4)_6OH_2$ [El Mhammedi et al. 2007]. The band observed at 1432 $cm^{-1}$ is due to the presence of a very small amount of calcium carbonate. At lower frequencies, two bands assigned to the phosphate ion are at 1032 $cm^{-1}$ and the low intensity band at 567 $cm^{-1}$ [Cao et al. 2010].

**X -Ray Diffraction (XRD)**

A change in the crystal structure of the polyvinyl alcohol on addition of silica nanoparticles and on increasing their concentration was studied by the XRD patterns. The polymer films were irradiated with x-ray and scanned at the rate of 0.02 A º with a range of angles 5 º to 90 º. Plots of intensity of the x ray diffracted by the composite versus two theta (angle) were observed to study the differences thus obtained.

**Sources of Error**

The instrument was calibrated to check the accuracy by running the XRD for corundum and comparing the results obtained with the standard patterns. The strain rate was kept small In order to obtain definitive peaks between the ranges of angles being worked on. A larger strain rate sometimes leads to fuzzy patterns as the time spent at each angle in the range to be observed is less.

The crystalline structure of polyvinyl alcohol is shown by the XRD pattern ( Figure 35). Strong peaks seen at angles of 30º, 40º, 50°,60° and 65° are a representation of the crystalline structure of PVA [Manias et al. 2001]. A change in the XRD pattern was

observed on the matrix (Figure 36). Peaks seen in the polymer matrix are not present in the XRD pattern of 39 wt.% silica.

However, a very strong peak is seen at an angle of 20° which was not seen the PVA pattern. The loss of the inherent structure of PVA on addition of silica is thus observed. The peak at angle of 20° (d spacing 4.44 A º) shows the possibility of exfoliated silica nanoparticles dispersed in the PVA matrix. On observing the wide angle X-Ray diffraction pattern for the polymer nanocomposite with a higher composition of silica nanoparticles (120 wt. %) the intensity of peak is at angle of 20° is further decreased (Figure 37).

This may be explained by the fact that as the amount of silica nanoparticles in the polymer matrix increases, polymer loses its crystalline structure and hence the intensity of the peak decreases [Yu et al. 2007]. Thus, it can be concluded that on increasing the concentration of silica nanoparticles in the polyvinyl alcohol matrix, the original crystal structure of the polymer is lost while the formation of exfoliated nanocomposite of silica and polyvinyl alcohol occurs as expected.

Also observed by this technique was the nanocomposite coated with calcium hydroxyapatite (Figure 38). The XRD pattern showed peaks at 25°, 35°, 40° and 60°. This pattern thus obtained confirmed the coating of the calcium hydroxyapatite on the surface of the nanocomposite [Ishikawa et al. 1993]. The pattern of calcium hydroxyapatite clearly showed a coating, with crystalline structure of the exfoliated nanocomposite that had lost its original structure.

Apart from using PVA as possible for the polymer matrix, we also worked with polyethylene oxide (PEO) and polycaprolactone (PCL). On casting the PEO/silica films, it was observed that with a minimum 39 wt. % silica nanoparticles the films obtained were brittle and hence no mechanical tests were performed. The primary reason for the brittle nature of films may be the poor linkage of the silica and the PEO matrix.

PCL/silica nanocomposites were also prepared by the modification of the silica nanoparticles. Silanol groups were introduced on the surface of silica and the films of PCL/ silica were casted and left for the solvent i.e. chloroform to evaporate. However, the

modulus and the strength of the films with 78.4% silica concentration were very low. Increasing the concentration of silica was not possible since the solution of PCL/ silica became viscous and silica could not be distributed homogeneously in the solution. Therefore, we constructed the PVA/silica nanocomposite.

# Conclusions

The change in mechanical properties and chemical structure of PVA on reinforcement with silica nanoparticles was studied by various techniques. It was observed that the modulus of the polymer matrix increased from 300MPa (10 wt. %) to 7.2GPa (120 wt. % of silica) while the ultimate tensile strength increased from 3.5MPa to 33MPa. The modulus and strength of the nanocomposite increased to 11GPa and 65MPa on coating with hydroxyapatite crystals. The mechanical properties of the nanocomposites were tested by both RSA and nanoindentation. The results obtained by both techniques were in agreement, thus PVA-silica nanocomposite is successfully constructed with high mechanical properties

The chemical characterization of nanocomposite showed effective cross-linking of the filler with the polymer with the filler being nearly homogeneously distributed throughout the polymer matrix. Thus problem of phase segregation occurring in the conventional nanocomposite systems was done away with by using the like natured filler and polymer.

However, the increasing concentration of silica in the nanocomposite from 78.4 wt. % to 120 wt.% made the polymer films brittle and thus limited the addition of silica nanoparticles. This ductile to brittle transition of the nanocomposite can be explained on the basis of decrease in the inter-particle distance and thus presence of some uncross-linked particles.

In order to achieve the ultimate aim of the research conducted, the nanocomposite was coated with calcium hydroxyapatite crystals to mimic the structure of bone. This coating further increased the modulus and strength of the composite on the order of human bone [Wall et al. 1979] i.e. a modulus of 12GPa and strength of 65MPa.

Therefore it can be concluded that nanocomposite of polyvinyl alcohol reinforced with silica is successfully constructed and should be tested for the growth of bone cells.

## Future Work

In order to use the nanocomposite constructed above as a scaffold for the reinforcement of bone, it has to be checked for the adhesion and differentiation of bone cells. The thickness of the nanocomposite has to be increased to few microns to construct a porous scaffold. The porous scaffold can be constructed by attaching functional groups such as polystyrene onto the nanocomposite surface and thus removing them using an organic solvent. This porous scaffold should then be dipped in media for the cell growth and be seeded with bone cells. The adhesion, growth and differentiation of cells should be monitored at regular intervals of time by conducting microscopic examination.

# References


1. Agag T, Koga T, Takeichi T. 2001. Studies on thermal and mechanical properties of polyimide–clay nanocomposites. Polymer 42(8):3399-408.
2. Asada M, Miura Y, Osaka A, Oukami K, Nakamura S. 1988. Hydroxyapatite crystal growth on calcium hydroxyapatite ceramics. Journal of Materials Science 23(9):3202-5.
3. Balasubramanian K, Burghard M. 2005. Chemically functionalized carbon nanotubes. Small 1(2):180-92.
4. Bandyopadhyay A, Sarkar M, Bhowmick A. 2005. Poly (vinyl alcohol)/silica hybrid nanocomposites by sol-gel technique: Synthesis and properties. Journal of Materials Science 40(19):5233-41.
5. Bonfield W. 1988. Hydroxyapatite-reinforced polyethylene as an analogous material for bone replacement. Annals of the New York Academy of Sciences 523: 173–7.
6. Bourlinos A, Bakandritsos A, Zboril R, Karakassides M, Trapalis C. 2007. Preparation of a water-dispersible carbon–silica composite derived from a silylated molecular precursor. Carbon 45(5):1108-11.
7. Briscoe B, Fiori L, Pelillo E. 1998. Nano-indentation of polymeric surfaces. Journal of Physics-London-D Applied Physics 31(19):2395-405.
8. Bull S. 2005. Nano-indentation of coatings. Journal of Physics-London-D Applied Physics 38(24):393-413.
9. Burr D. 2002. Bone material properties and mineral matrix contributions to fracture risk or age in women and men. Journal of Musculoskeletal and Neuronal Interactions 2(3):201-4.
10. Burr D. 2002. The contribution of the organic matrix to bone's material properties. Bone 31(1):8-11.

11. Cao SW, Zhu YJ, Wu J, Wang KW, Tang QL.2010. Preparation and Sustained-Release Property of Triblock Copolymer/Calcium Phosphate Nanocomposite as Nanocarrier for Hydrophobic Drug. Nanoscale research letters 5(4):781-85.
12. Chatterji S, Jeffery JW. 1968. Changes in structure of human bone with age. Nature 219:482-4.
13. Chen TK, Tien YI, Wei KH. 2000. Synthesis and characterization of novel segmented polyurethane/clay nanocomposites. Polymer 41(4):1345-53.
14. Christenson EM, Anseth KS, Beucken JJJP, Chan CK, Ercan B, Jansen JA, Laurencin CT, Li WJ, Murugan R, Nair LS. 2007. Nanobiomaterial applications in orthopedics. Journal of Orthopaedic Research 25(1): 11–22.
15. Colo SM, Herh PKW, Roye N, Larsson M. 2004. Rheology and the texture of pharmaceutical and cosmetic semisolids. American Laboratory 36:26-35.
16. Costa VC, Costa HS, Vasconcelos WL, Pereira MM, Oréfice RL, Mansur HS. 2007. Preparation of hybrid biomaterials for bone tissue engineering. Materials Research 10(1):21-6.
17. Currey J. 1984. Effects of differences in mineralization on the mechanical properties of bone. Philosophical Transactions of the Royal Society of London. Series B, Biological Sciences 304(1121):509-18.
18. Dufresne A, Paillet M, Putaux J, Canet R, Carmona F, Delhaes P, Cui S. 2002. Processing and characterization of carbon nanotube/poly (styrene-co-butyl acrylate) nanocomposites. Journal of Materials Science 37(18):3915-23.
19. Eichhorn S, Baillie C, Zafeiropoulos N, Mwaikambo L, Ansell M, Dufresne A, Entwistle K, Herrera-Franco P, Escamilla G, Groom L. 2001. Review: Current international research into cellulosic fibres and composites. Journal of Materials Science 36(9):2107-31.
20. El Mhammedi MA, Bakasse M, Chtaini A. 2007. Voltammetric detection of diquat at the carbon paste electrode containing a $Ca_{10}$ $(PO_4)_6$ $(OH)_2$. Leonardo Electronic Journal of Practices and Technologies 10:1-12.

21. Fischer-Cripps AC. 2006. Critical review of analysis and interpretation of nanoindentation test data. Surface and Coatings Technology 200(14-15):4153-65.
22. Fornes TD, Paul DR. 2003. Modeling properties of nylon 6/clay nanocomposites using composite theories. Polymer 44(17):4993-5013.
23. Fu X, Qutubuddin S. 2000. Synthesis of polystyrene–clay nanocomposites. Materials Letters 42(1-2):12-5.
24. Garcia-Lopez D, Picazo O, Merino J, Pastor J. 2003. Polypropylene-clay nanocomposites: effect of compatibilizing agents on clay dispersion. European Polymer Journal 39(5):945-50.
25. Gasser B. 2000. About composite materials and their use in bone surgery. Injury 31(4):48-53.
26. Geng H, Rosen R, Zheng B, Shimoda H, Fleming L, Liu J, Zhou O. 2002. Fabrication and properties of composites of poly (ethylene oxide) and functionalized carbon nanotubes. Advanced Materials 14(19):1387-90.
27. Gojny FH, Nastalczyk J, Roslaniec Z, Schulte K. 2003. Surface modified multi-walled carbon nanotubes in CNT/epoxy-composites. Chemical Physics Letters 370(5-6):820-4.
28. Hollinger J, Brekke J, Gruskin E, Lee D. 1996. Role of bone substitutes. Clinical Orthopaedics and Related Research March (324):55-65.
29. Hong Z, Zhang P, Liu A, Chen L, Chen X, Jing X. 2007. Composites of poly (lactide-co-glycolide) and the surface modified carbonated hydroxyapatite nanoparticles. Journal of Biomedical Materials Research Part A (3): 515–22.
30. Hong Z, Zhang P, He C, Qiu X, Liu A, Chen L, Chen X, Jing X. 2005. Nano-composite of poly (L-lactide) and surface grafted hydroxyapatite: Mechanical properties and biocompatibility. Biomaterials 26(32): 6296-304.
31. Hsueh CH. 2000. Young's modulus of unidirectional discontinuous-fibre composites. Composites Science and Technology 60(14):2671-80.

32. Hu Q, Li B, Wang M, Shen J. 2004. Preparation and characterization of biodegradable chitosan/hydroxyapatite nanocomposite rods via in situ hybridization: a potential material as internal fixation of bone fracture. Biomaterials 25(5):779-85.
33. Ikada Y. 2006. Challenges in tissue engineering. Journal of the Royal Society Interface 3(10): 589-601.
34. Ishikawa K, Ducheyne P, Radin S. 1993. Determination of the Ca/P ratio in calcium-deficient hydroxyapatite using X-ray diffraction analysis. Journal of Materials Science: Materials in Medicine 4(2):165-8.
35. Jang J, Park H. 2002. Formation and structure of polyacrylamide-silica nanocomposites by sol-gel process. Journal of Applied Polymer Science 83(8): 1817–23.
36. Kim JA, Seong DG, Kang TJ, Youn JR. 2006. Effects of surface modification on rheological and mechanical properties of CNT/epoxy composites. Carbon 44(10):1898-905.
37. Lin Y, Zhou B, Fernando KAS, Liu P, Allard LF, Sun YP. 2003. Polymeric carbon nanocomposites from carbon nanotubes functionalized with matrix polymer. Macromolecules 36(19):7199-204.
38. Liu Q, Wijn de JR, Blitterswijk van CA. 1997. Nano-apatite/polymer composites: Mechanical and physicochemical characteristics. Biomaterials 18(19):1263-70.
39. Ma J, Qi Z, Hu Y. 2001. Synthesis and characterization of polypropylene/clay nanocomposites. Journal of Applied Polymer Science 82(14): 3611–7.
40. Mamedov AA, Kotov NA, Prato M, Guldi DM, Wicksted JP, Hirsch A. 2002. Molecular design of strong single-wall carbon nanotube/polyelectrolyte multilayer composites. Nature Materials 1(3):190-4.
41. Manias E, Touny A, Wu L, Strawhecker K, Lu B, Chung T. 2001. Polypropylene/montmorillonite nanocomposites. Review of the synthetic routes and materials properties. Chemistry of Materials 13(10):3516-23.

42. Marra KG, Szem JW, Kumta PN, DiMilla PA, Weiss LE. 1999. In vitro analysis of biodegradable polymer blend/hydroxyapatite composites for bone tissue engineering. Journal of Biomedical Materials Research 47(3):324-35.
43. Martin B. 1993. Aging and strength of bone as a structural material. Calcified Tissue International 53(1):34-40.
44. Martin TJ, Sims NA. 2005. Osteoclast-derived activity in the coupling of bone formation to resorption. Trends in Molecular Medicine 11(2):76-81.
45. McNally T, Pötschke P, Halley P, Murphy M, Martin D, Bell SEJ, Brennan GP, Bein D, Lemoine P, Quinn JP. 2005. Polyethylene multiwalled carbon nanotube composites. Polymer 46(19):8222-32.
46. Mitchell CA, Bahr JL, Arepalli S, Tour JM, Krishnamoorti R. 2002. Dispersion of functionalized carbon nanotubes in polystyrene. Macromolecules 35(23):8825-30.
47. Mukherjee M, Das C, Kharitonov A, Banik K, Mennig G, Chung T. 2006. Properties of syndiotactic polystyrene composites with surface modified short kevlar fiber. Materials Science & Engineering A 441(1-2):206-14.
48. Murugan R, Ramakrishna S. 2005. Development of nanocomposites for bone grafting. Composites Science and Technology 65(15-16):2385-406.
49. Nadagouda MN, Varma RS. 2007. Microwave-assisted synthesis of crosslinked poly (vinyl alcohol) nanocomposites comprising single-walled carbon nanotubes, multi-walled carbon nanotubes, and buckminsterfullerene. Macromolecular Rapid Communications 28(7): 842–7.
50. Nuriel S, Liu L, Barber A, Wagner H. 2005. Direct measurement of multiwall nanotube surface tension. Chemical Physics Letters 404(4-6):263-6.
51. Park J, Choi Y, Kim KB, Chung H, Sohn D. 2008. Aggregation processes of a weak polyelectrolyte, poly (allylamine) hydrochloride. Bulletin-Korean Chemical Society 29 (1): 104-10.

52. Park SY, Lee SW, Oh TJ. 2006. Preparation and properties of a poly (2-cyano-1, 4-phenylene terephthalamide)/layered silicate nanocomposite. Journal of Applied Polymer Science 102(1):640-5.
53. Patwardhan SV. 2003. Silicification and biosilicification: The role of macromolecules in bioinspired silica synthesis.
54. Peng Z, Kong LX, Li SD. 2005. Thermal properties and morphology of a poly (vinyl alcohol)/silica nanocomposite prepared with a self-assembled monolayer technique. Journal of Applied Polymer Science 96(4): 1436–42.
55. Peng Z, Kong LX, Li SD. 2005. Non-isothermal crystallisation kinetics of self-assembled polyvinylalcohol/silica nano-composite. Polymer 46 (6): 1949-55.
56. Rho JY, Kuhn-Spearing L, Zioupos P. 1998. Mechanical properties and the hierarchical structure of bone. Medical Engineering and Physics 20(2):92-102.
57. Ribelles JLG, Sebastià JM, Soler RM, Pradas MM, Greus AR, Antón JJS. 1991. On the dynamic mechanical behavior of poly (ethyl methacrylate) reinforced with kevlar fibers. Journal of Applied Polymer Science 42(6):1647-57.
58. Riboldi SA, Sampaolesi M, Neuenschwander P, Cossu G, Mantero S. 2005. Electrospun degradable polyesterurethane membranes: potential scaffolds for skeletal muscle tissue engineering. Biomaterials 26(22):4606-15.
59. Rodan GA, Martin TJ. 1981. Role of osteoblasts in hormonal control of bone resorption—a hypothesis. Calcified Tissue International 33(1):349-51.
60. Rouse JH, Lillehei PT. 2003. Electrostatic assembly of polymer/single walled carbon nanotube multilayer films. Nano Letters 3(1):59-62.
61. Salehi-Mobarakeh H, Ait-Kadi A, Brisson J. 1996. Improvement of mechanical properties of composites through polyamide grafting onto kevlar fibers. Polymer Engineering & Science 36(6): 778–85.
62. Strawhecker K, Manias E. 2003. Crystallization behavior of poly (ethylene oxide) in the presence of $Na^+$ montmorillonite fillers. Chemical Materials 15(4):844-9.

63. Takayanagi M, Katayose T. 1983. Syntheses and characterization of N-grafted poly (p-phenylene terephthalamide). Journal of Polymer Science: Polymer Chemistry Edition 21(1):31-9.
64. Tas ACK. 2000. Synthesis of biomimetic Ca-hydroxyapatite powders at 373C in synthetic body fluids. Biomaterials 21:1429-38.
65. Teitelbaum SL. 2000. Bone resorption by osteoclasts. Science 289(5484):1504-8.
66. Van Zyl WE, García M, Schrauwen BAG, Kooi BJ, De Hosson JTM, Verweij H. 2002. Hybrid polyamide/silica nanocomposites: Synthesis and mechanical testing. Macromolecular Materials and Engineering 287(2):106-10.
67. Wall JC, Chatterji SK, Jeffery JW. 1979. Age-related changes in the density and tensile strength of human femoral cortical bone. Calcified Tissue International 27(1):105-8.
68. Wang H, Liu C, Shi P, Xu B. 2005. Design and micro mechanical properties of nano-$SiO_2$ strengthened composite coatings towards remanufacturing. Journal of Central South University of Technology 12(2):190-4.
69. Wang M, Pramoda K, Goh SH. 2006. Enhancement of interfacial adhesion and dynamic mechanical properties of poly (methyl methacrylate)/multiwalled carbon nanotube composites with amine-terminated poly (ethylene oxide). Carbon 44(4):613-7.
70. Wang X, Shen X, Li X, Mauli Agrawal C. 2002. Age-related changes in the collagen network and toughness of bone. Bone 31(1):1-7.
71. Webb AR, Kumar VA, Ameer GA. 2007. Biodegradable poly (diol citrate) nanocomposite elastomers for soft tissue engineering. Journal of Materials Chemistry 17(9):900-6.
72. With G, Dijk H, Hattu N, Prijs K. 1981. Preparation, microstructure and mechanical properties of dense polycrystalline hydroxy apatite. Journal of Materials Science 16(6):1592-8.

73. Wu CL, Zhang MQ, Rong MZ, Friedrich K. 2005. Silica nanoparticles filled polypropylene: Effects of particle surface treatment, matrix ductility and particle species on mechanical performance of the composites. Composites Science and Technology 65(3-4):635-45.
74. Yang F, Nelson GL. 2004. PMMA/silica nanocomposite studies: Synthesis and properties. Journal of Applied Polymer Science 91(6): 3844–50.
75. Yang F, Ou Y, Yu Z. 1998. Polyamide 6/silica nanocomposites prepared by in situ polymerization. Journal of Applied Polymer Science 69(2):355-61.
76. Yu T, Lin J, Xu J, Chen T, Lin S, Tian X. 2007. Novel polyacrylonitrile/Na-MMT/silica nanocomposite: Co-incorporation of two different form nano materials into polymer matrix. Composites Science and Technology 67(15-16):3219-25.
77. Zeng K, Chiu CH. 2001. An analysis of load–penetration curves from instrumented indentation. Acta Materialia 49(17):3539-51.
78. Zeng Q, Yu A, Lu G, Paul D. 2005. Clay-based polymer nanocomposites: Research and commercial development. Journal of Nanoscience and Nanotechnology 5(10):1574-92.
79. Zhang X, Liu T, Sreekumar T, Kumar S, Moore VC, Hauge RH, Smalley RE. 2003. Poly (vinyl alcohol)/SWCNT composite film. Nano Letters 3(9):1285-8.
80. Structure of Human Bone.http://www.sciencelearn.org.nz/Contexts/Ceramics/Sci-Media/Images/Human-bone-structure accessed on May 5 2011.

**Table 1: Review of nanocomposites used for bone reconstruction**

| Nanocomposite | Modulus (GPa) | Tensile strength(MPa) |
|---|---|---|
| HA/PAA [Liu et al. 1997] | $(79.2 \pm 3.3) * 10^{-3}$ | 6.0 ±0.3 |
| HA/PCL/PLGA [Marra et al. 1999] | $(12.5 \pm 3.2) * 10^{-3}$ | 0.51 ± 0.08 |
| MMA/Cellulose [Eichhorn et al. 2001] | (1.02)±0.39 | 92±32 |
| HA/Alginate/Collagen [Zhang et al. 2003] | $(350) * 10^{-3}$ | 23 |
| Chitosan/HA [Hu et al. 2004] | 3.4 | 84 |
| DegraPol® [Riboldi et al. 2005] | $(10.15) * 10^{-3}$ | 2.52 |
| PLLA/g-HA [Hong et al. 2005] | 3.7–4 | 75 |
| PLGA/g-cHA [Hong et al. 2007] | 3.7 | 75 |
| PLLA/PDC [Webb et al. 2007] | $(85) * 10^{-3}$ | 13 |

**Table 2: Composition of simulating body fluid [Tas 1998]**

| Reagent | Amount (g/l) |
|---|---|
| Sodium Chloride | 6.547 |
| Sodium Bicarbonate | 2.268 |
| Potassium Chloride | 0.373 |
| Disodium Hydrogen Phosphate dihydrate | 0.178 |
| Magnesium Chloride hexahydrate | 0.305 |
| Calcium Chloride dihydrate | 0.368 |
| Sodium Sulphate | 0.071 |
| Trishydroxymethyl amino methane | 6.057 |

**Table 3: Ultimate Tensile Strength of nanocomposite**

| **Concentration of silica in nanocomposite (wt. %)** | **Ultimate tensile strength obtained from RSA (MPa)** |
|---|---|
| 0 | 3.7±0.3 |
| 39 | 6±0.19 |
| 60 | 25±0.04 |
| 78.4 | 46±0.9 |
| 120 | 35±0.8 |
| 120 (Hydroxyapatite coated) | 65±0.67 |

**Table 4: Comparison of the modulus obtained by RSA, Nanoindentation, Stress-Strain Curve and theoretical calculations**

| Concentration of silica in nanocomposite (wt. %) | Modulus calculated from RSA (GPa) | Modulus calculated from Nanoindentation (GPa) | Modulus calculated from stress-strain curve (GPa) | Modulus calculated from Halpin Tsai |
|---|---|---|---|---|
| 0 | 0.3±0.10 | 0.3±0.13 | 0.3±0.19 | - |
| 39 | 3.22±0.22 | 3.4±0.14 | 3±0.22 | 4.0 |
| 60 | 4.87±0.29 | 4.8±0.09 | 5±0.18 | 5.2 |
| 78.4 | 6.65±0.31 | 6.8±0.29 | 6.5±0.12 | 7.0 |
| 120 | 7.2±0.24 | 8.1±0.19 | 8±0.16 | 8.0 |
| 120 (Hydroxyapatite coated) | 11.5±0.11 | 11.8±0.23 | 13.6±0.25 | 12.8 |

**Table 5: Theoretical hardness of the nanocomposite**

| **Concentration of Silica in nanocomposite (wt. %)** | **Theoretical Hardness (GPa)** |
|---|---|
| 0 | 0.357 |
| 39 | 1.34 |
| 60 | 0.339 |
| 78.4 | 0.312 |
| 120 | 0.276 |
| 120 (Hydroxyapatite coated) | 0.403 |

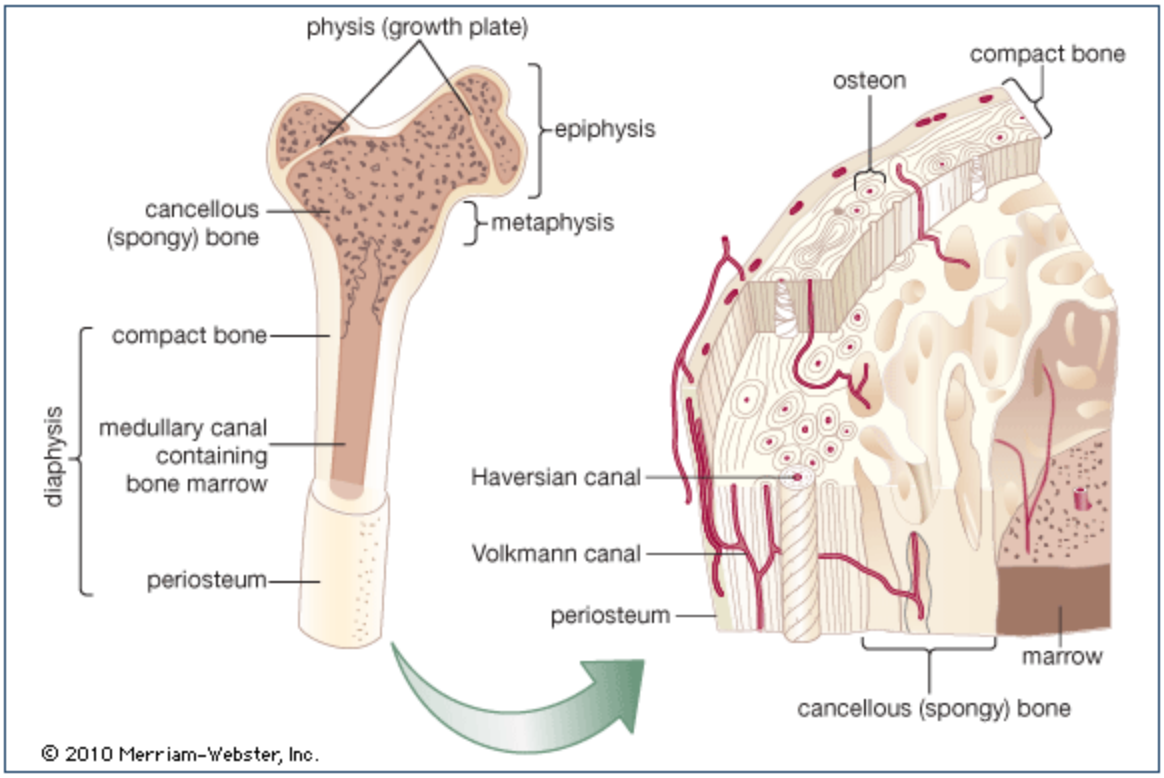


**Figure 1: Structure of Human Bone**

**[**http://www.sciencelearn.org.nz/Contexts/Ceramics/Sci-Media/Images/Human-bone-structure**]**

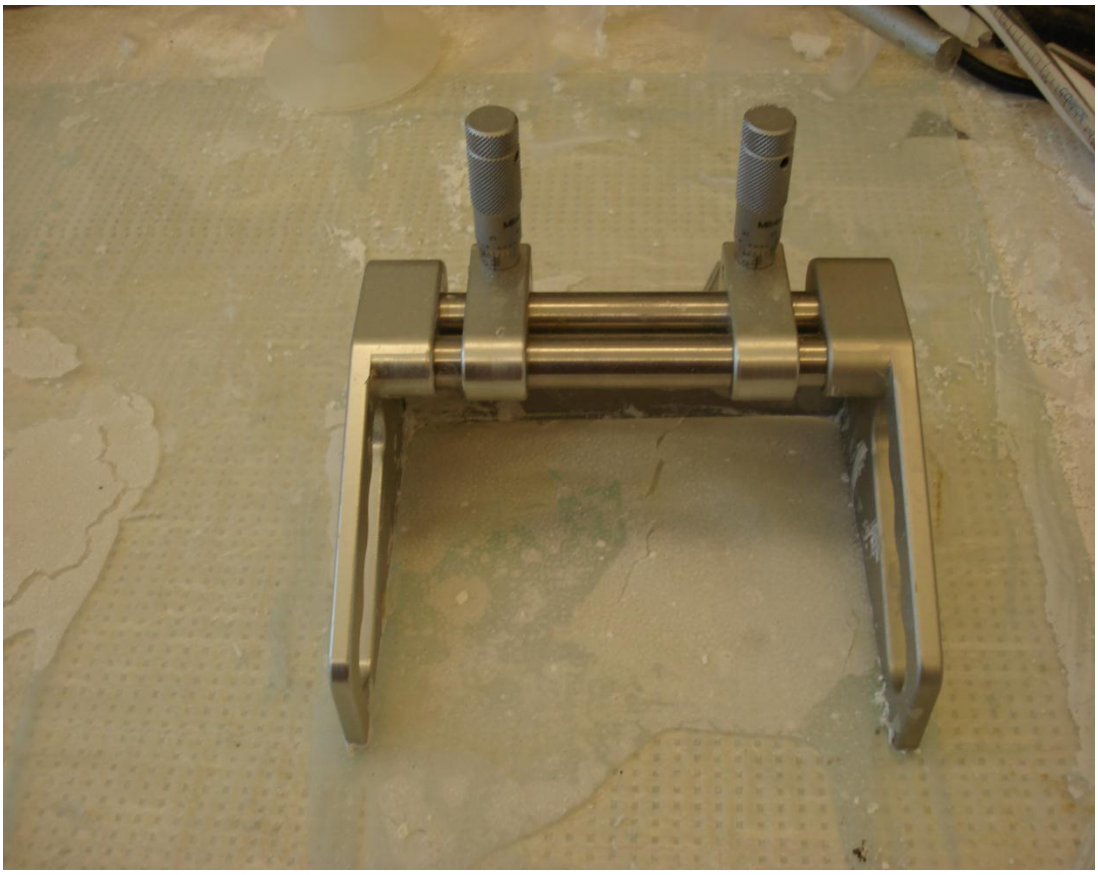

**Figure 2: Drawbar coater used for polymer film casting**

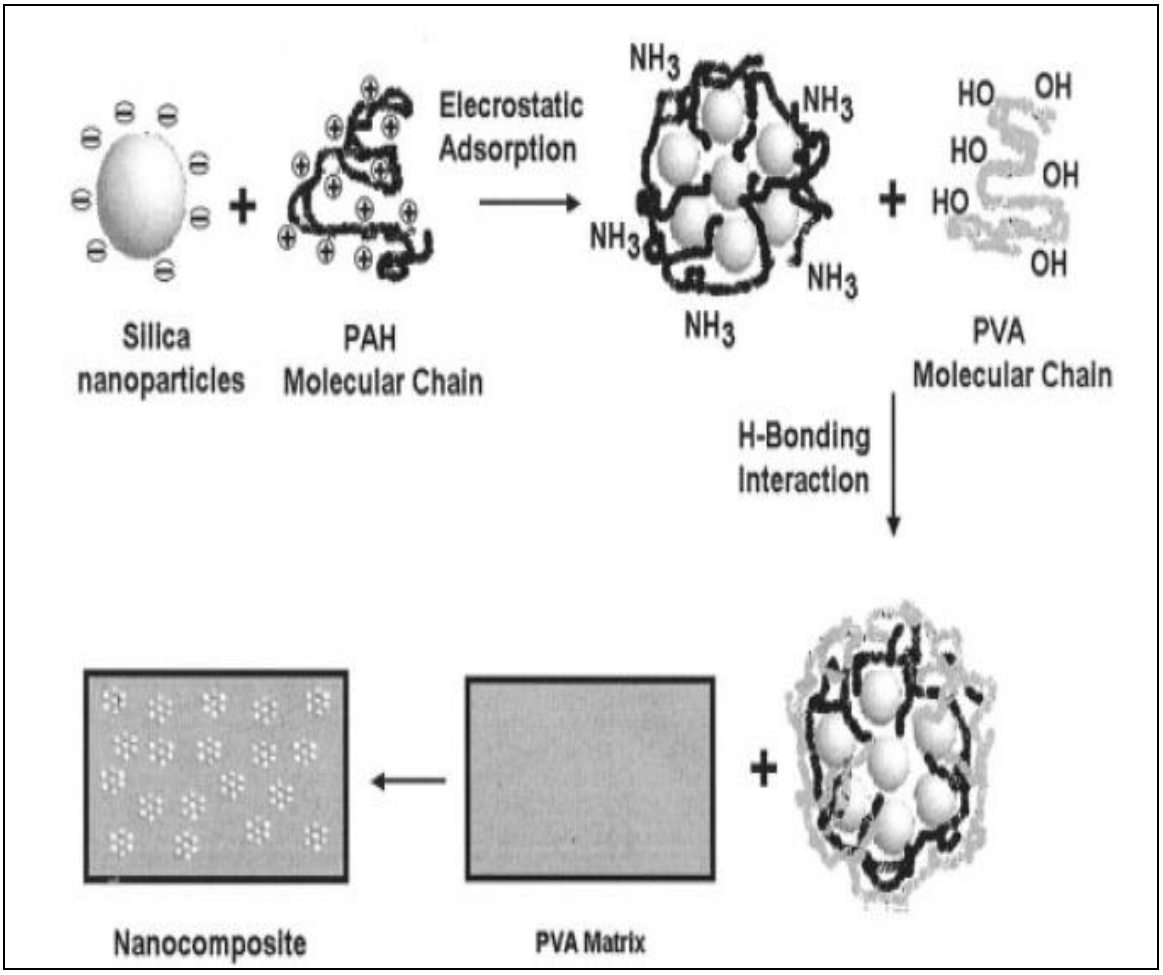


**Figure 3: Schematic of nanocomposite formation [Peng et al. 2005]**

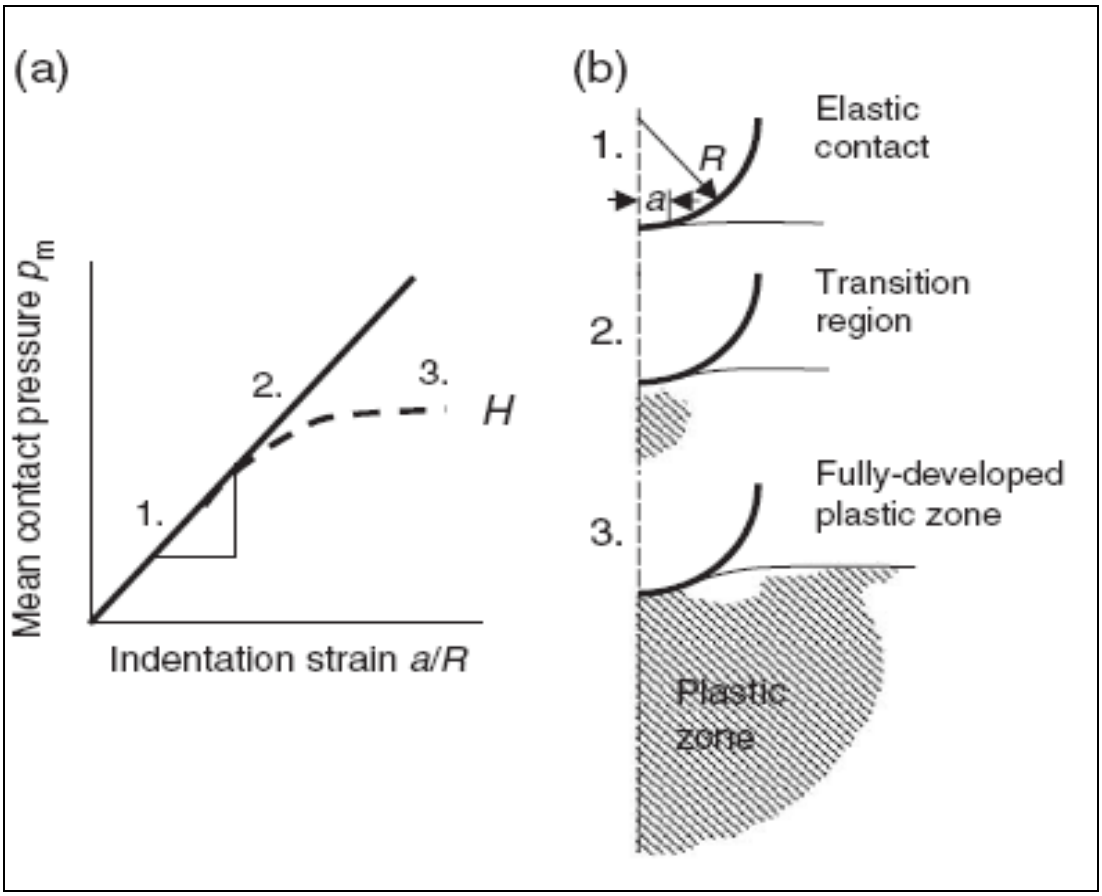


**Figure 4: Mechanics of Nanoindentation [Fischer-Cripps 2006]**

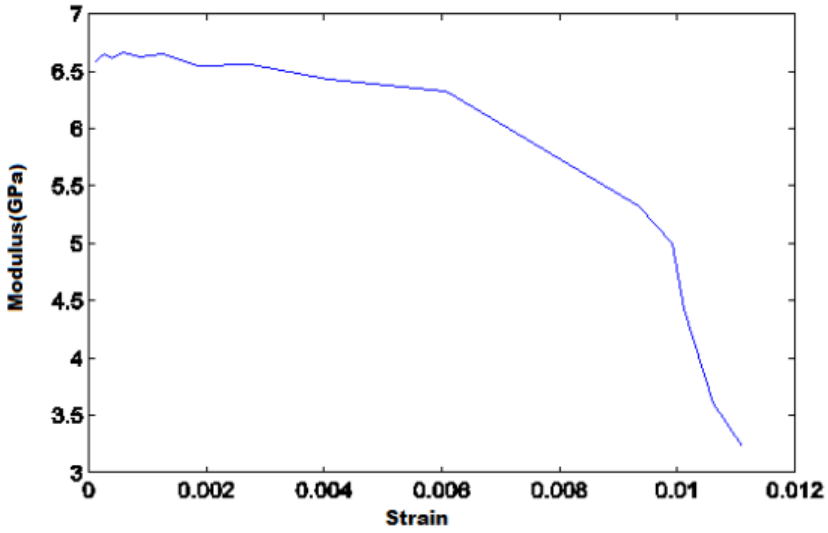


**Figure 5: Strain-sweep curve of the nanocomposite (silica 78.4 wt. %)**

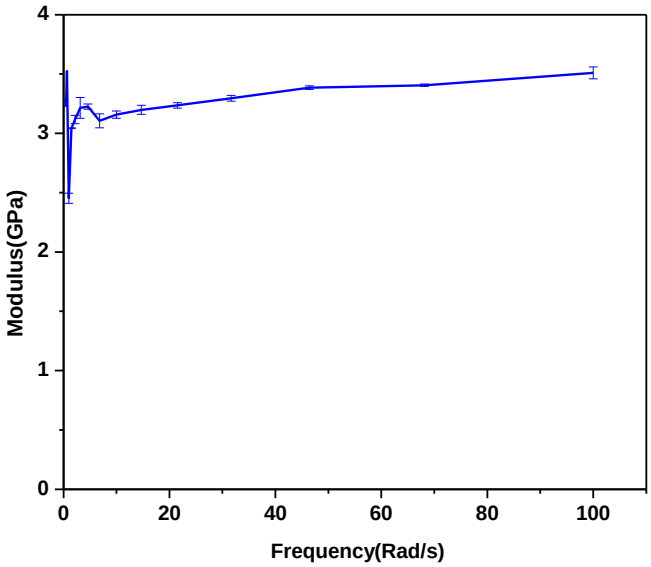


**Figure 6: Bulk Modulus of nanocomposite (silica 39 wt. %) versus Frequency**

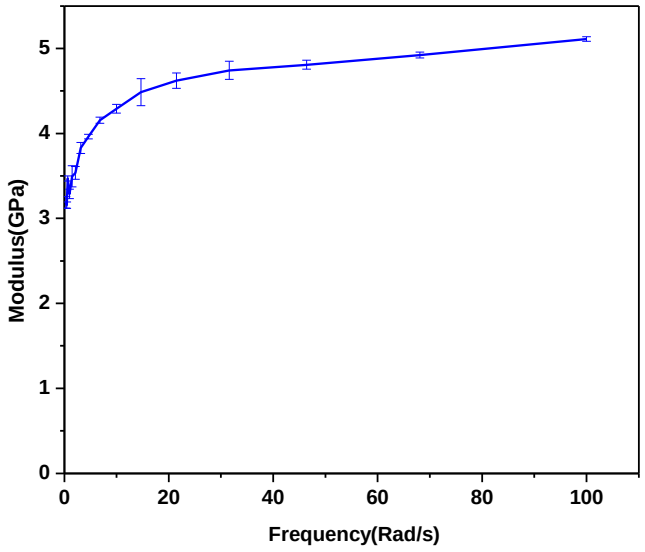


**Figure 7: Bulk Modulus of nanocomposite (silica 60 wt. %) versus Frequency**

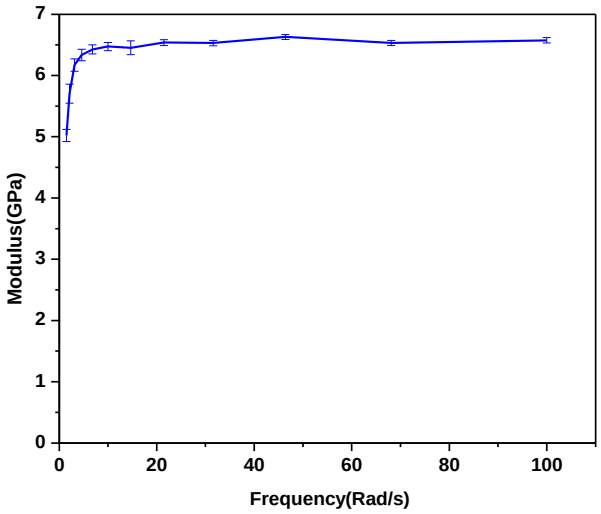


**Figure 8: Bulk Modulus of nanocomposite (silica 78.4 wt. %) versus Frequency**

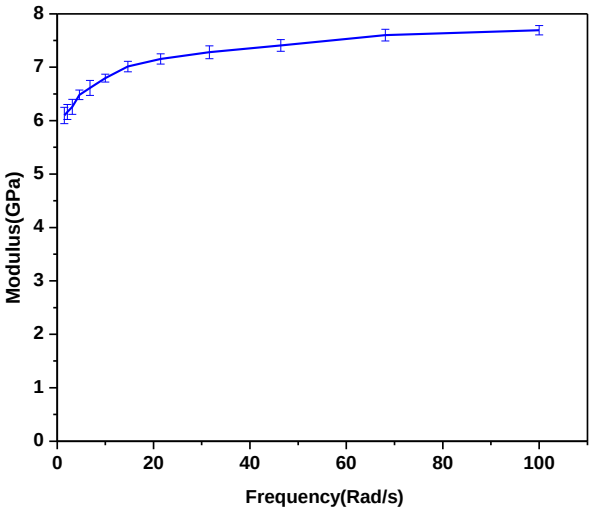


**Figure 9: Bulk Modulus of nanocomposite (silica 120wt. %) versus Frequency**

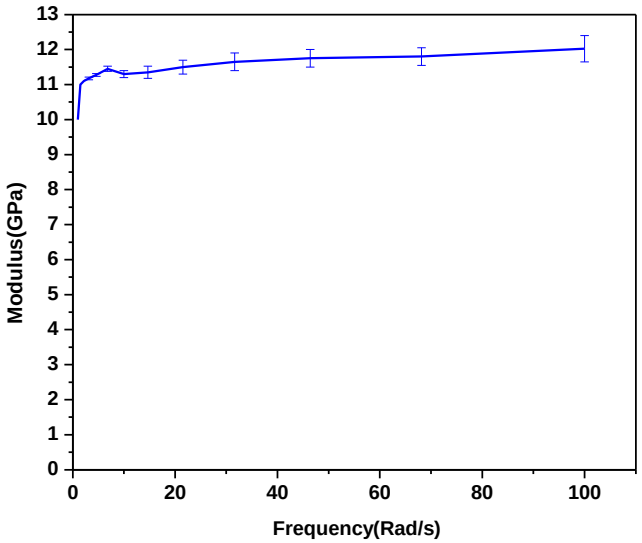


**Figure 10: Bulk Modulus of nanocomposite (silica 120 wt. % coated with calcium hydroxyapatite) versus Frequency**

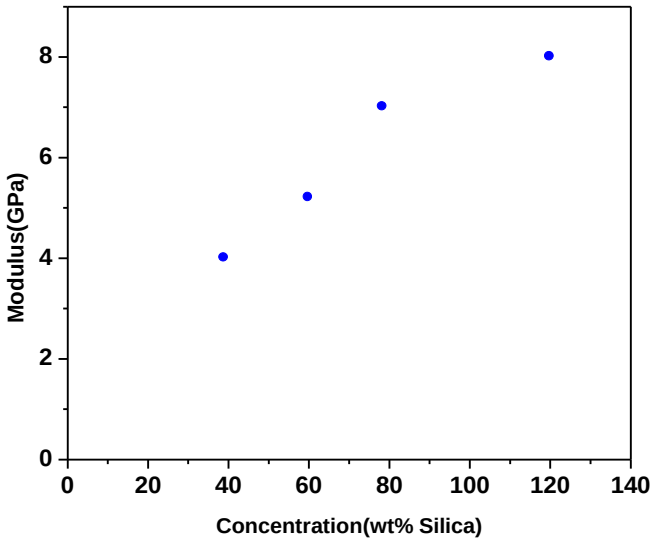


**Figure 11: Bulk Modulus of nanocomposite versus silica concentration**

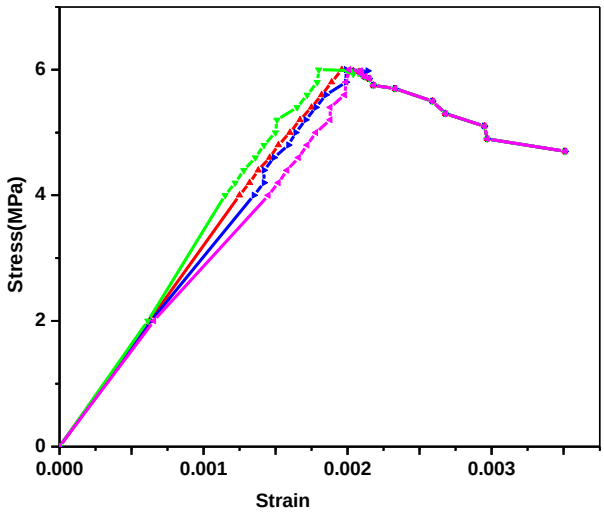


**Figure 12: Stress-Strain curve for nanocomposite (silica 39 wt. %)**

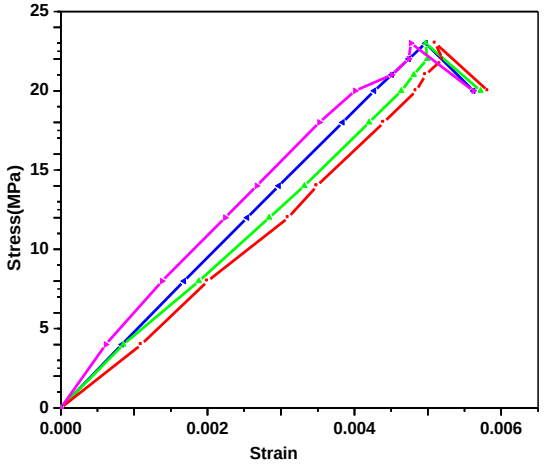


**Figure13: Stress-Strain curve for nanocomposite (silica 60 wt. %)**

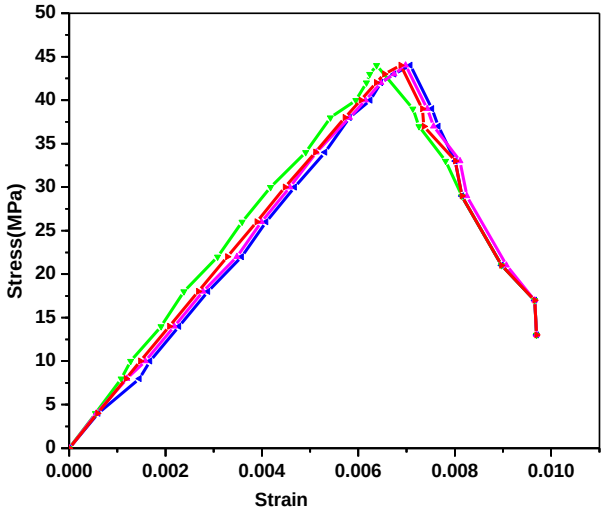


**Figure14: Stress-Strain curve for nanocomposite (silica 78.4wt. %)**

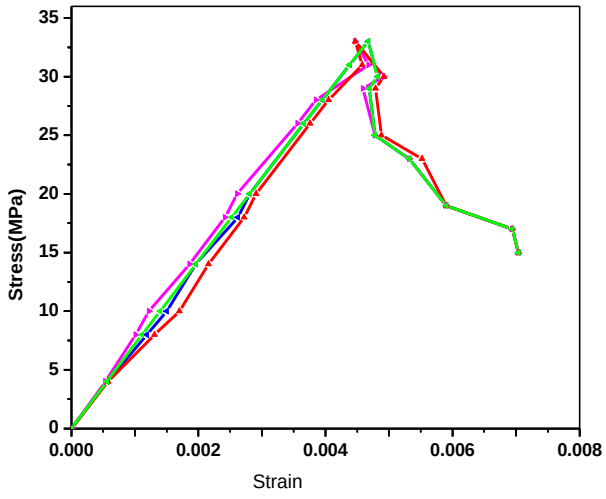


**Figure15: Stress-Strain curve for nanocomposite (silica 120wt. %)**

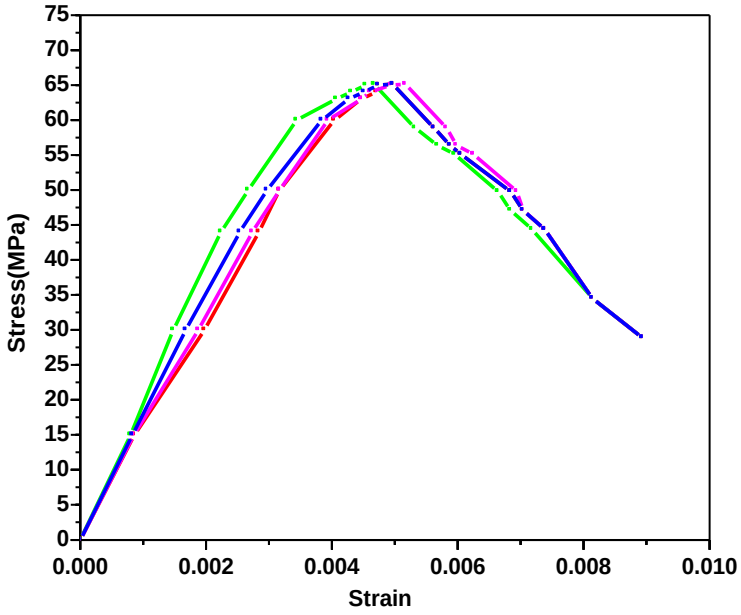


**Figure 16: Stress-Strain curve for nanocomposite (silica 120 wt. %) coated with apatite crystals.**

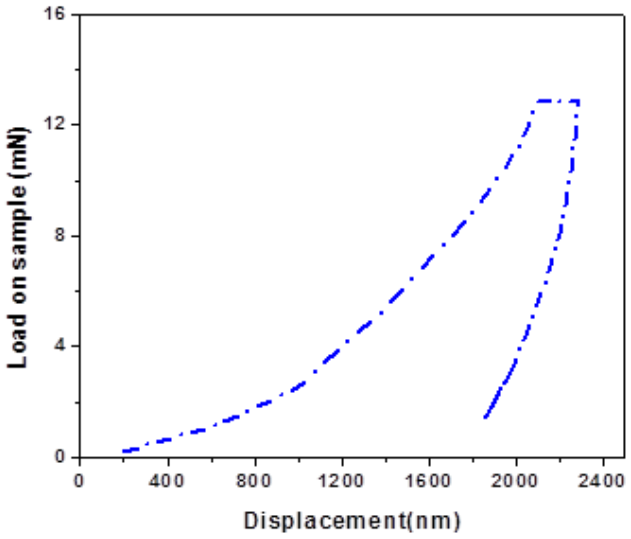


**Figure 17: Loading-Unloading curve of the nanocomposite (silica 39 wt. %)**

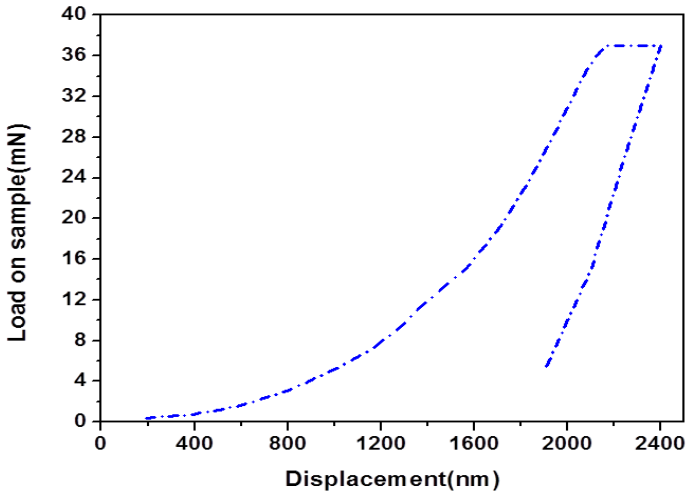


**Figure 18: Loading-Unloading curve of the nanocomposite (silica 60 wt. %)**

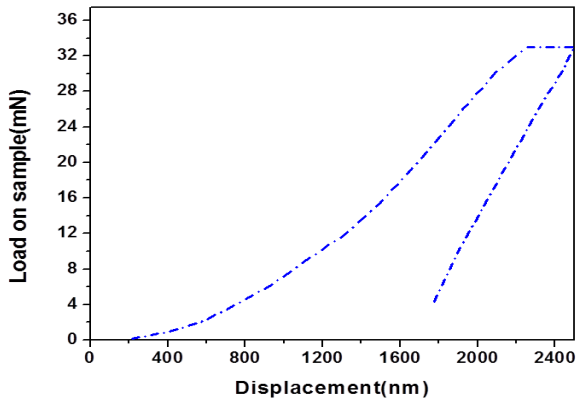


**Figure 19: Loading-Unloading curve of the nanocomposite (silica 78.4 wt. %)**

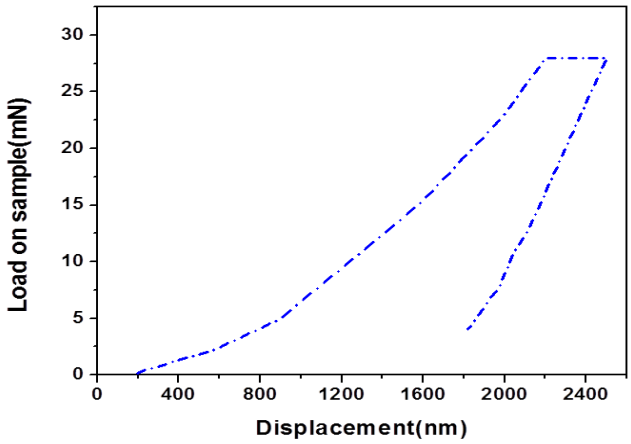


**Figure 20: Loading-Unloading curve of the nanocomposite (silica 120 wt. %)**

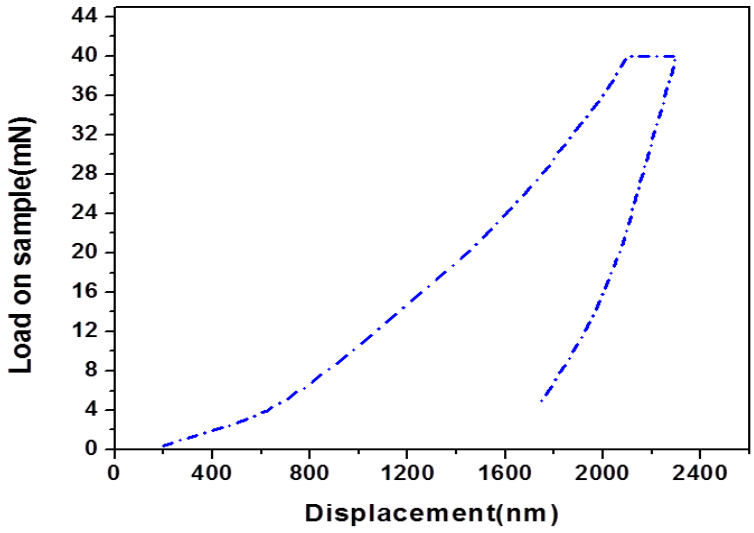


**Figure 21: Loading-Unloading curve for nanocomposite 120 wt. % silica coated with calcium hydroxyapatite**

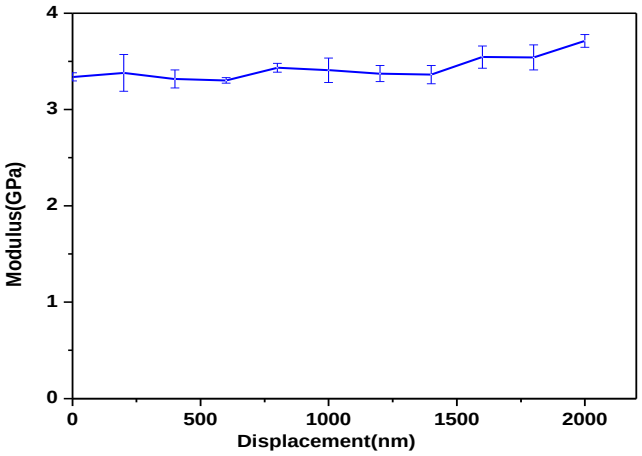


**Figure 22: Modulus of nanocomposite (silica 39 wt. %)**

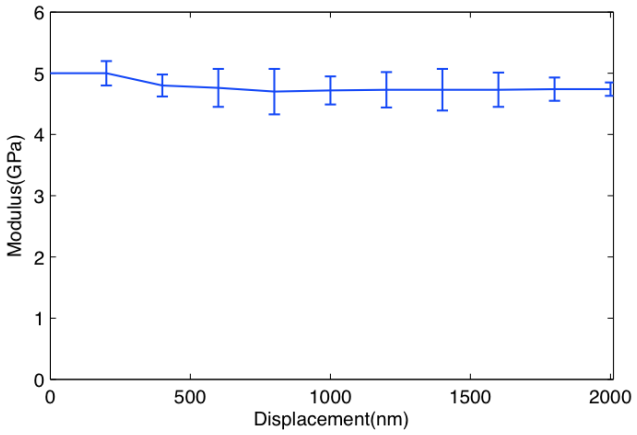


**Figure 23: Modulus of nanocomposite (silica 60 wt. %)**

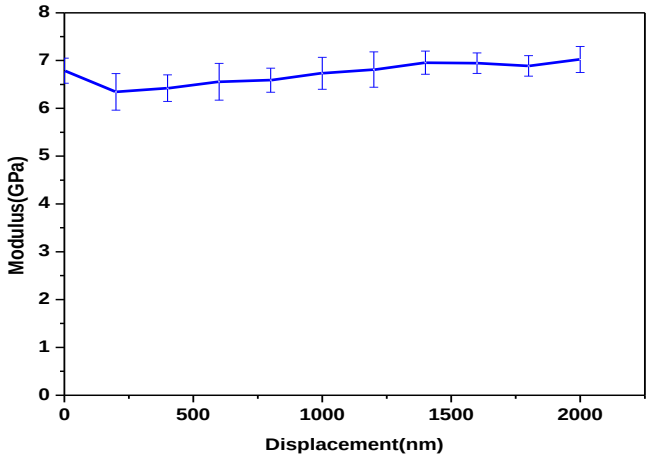


**Figure 24: Modulus of nanocomposite (silica 78.4 wt. %)**

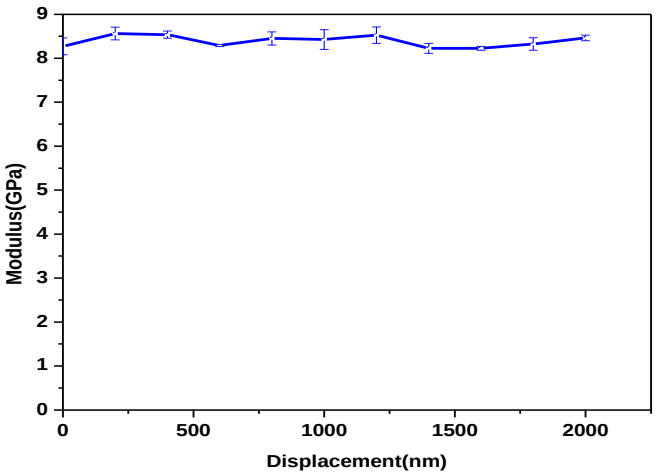


**Figure 25: Modulus of nanocomposite (silica 120 wt. %)**

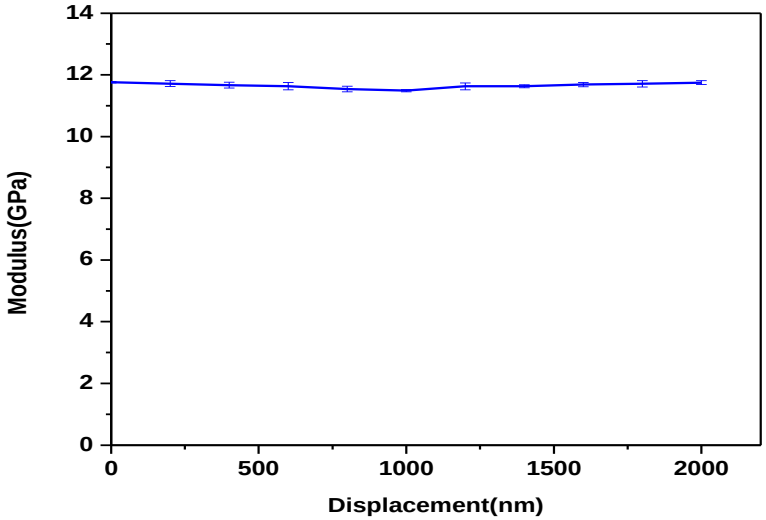


**Figure 26: Modulus of nanocomposite (silica 120 wt. %) coated with calcium hydroxyapatite**

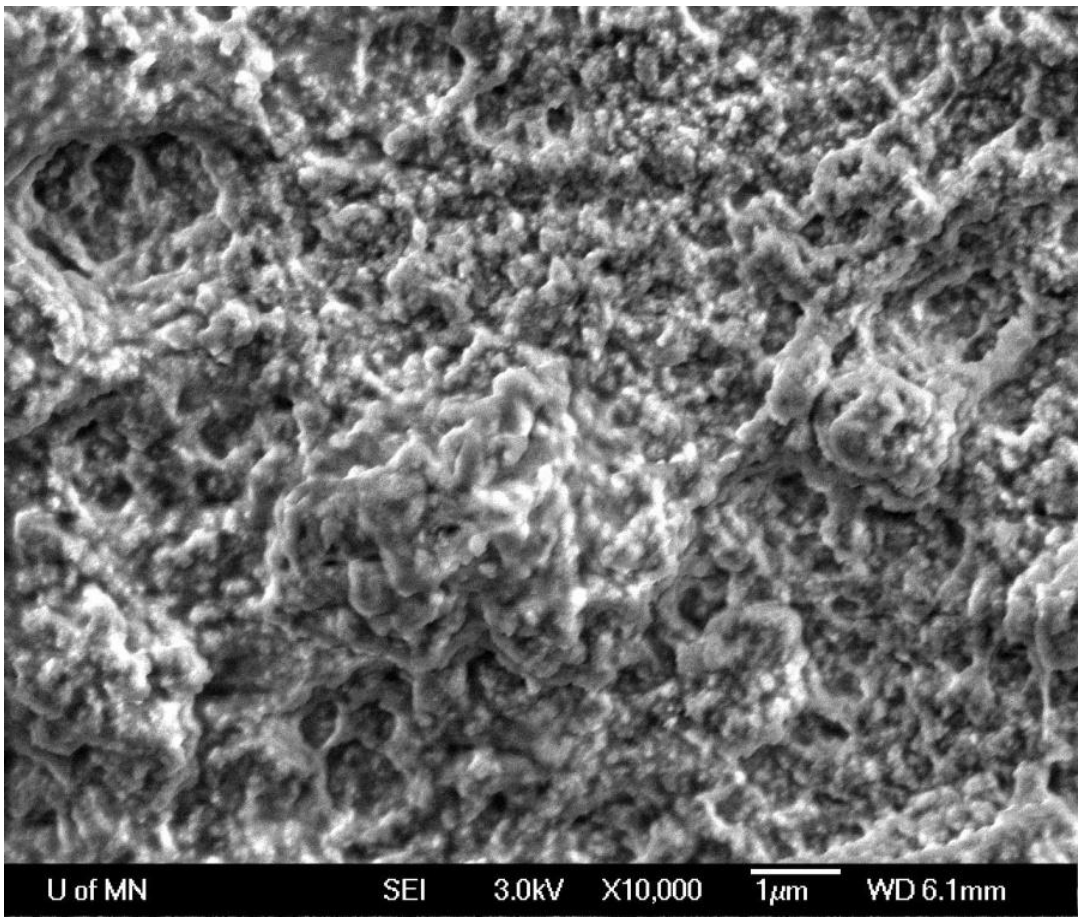


**Figure 27: SEM image of cross-linked nanocomposite (silica 78.4wt. %)**

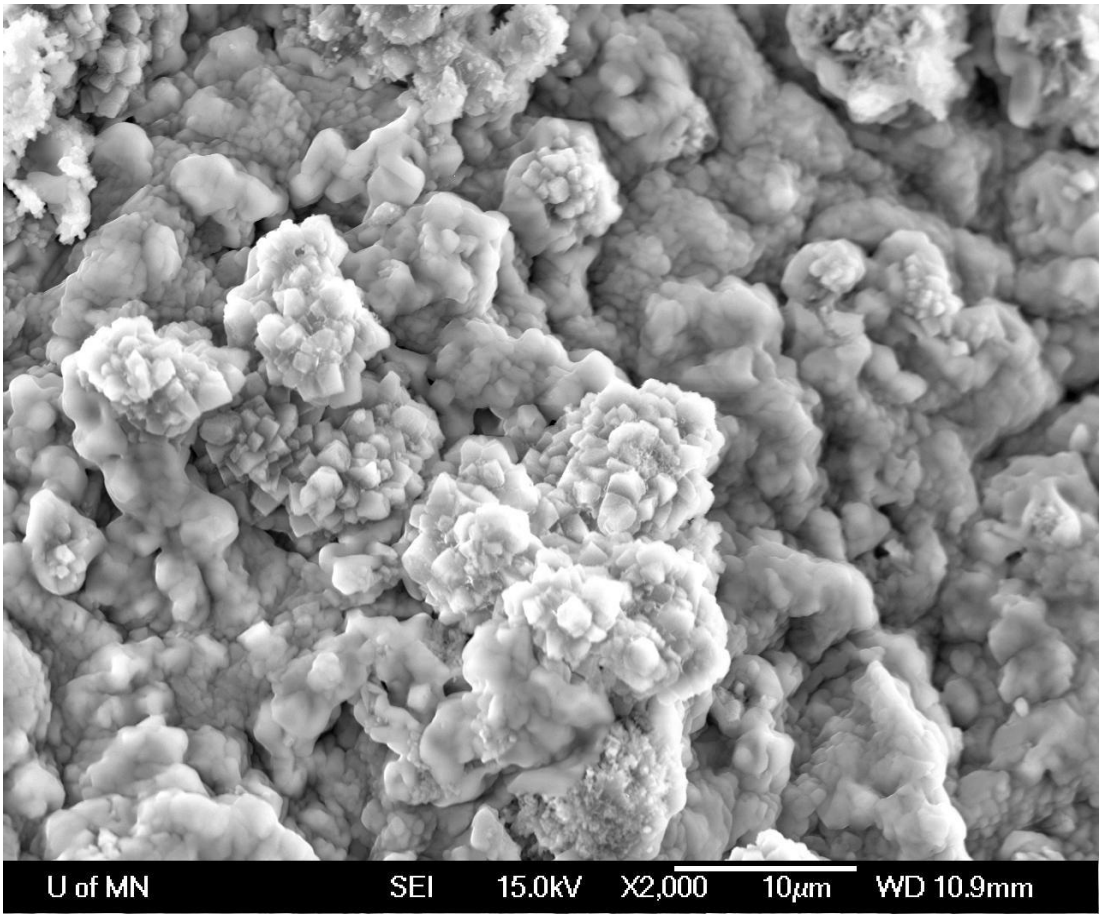


**Figure 28: SEM image showing increase in cross-linkage on increasing silica (120 wt. %) in nanocomposite**

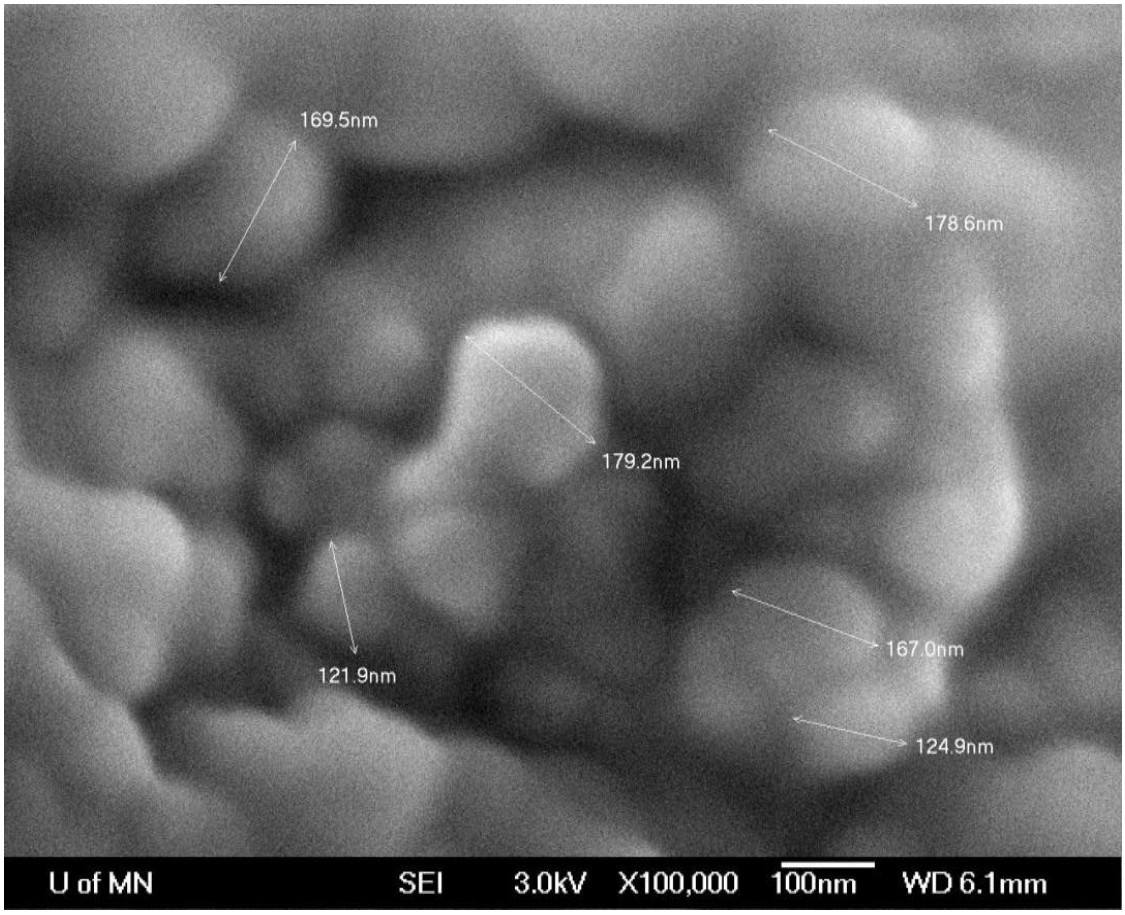


**Figure 29: SEM image of silica nanoparticles size in nanocomposite (silica 120 wt. %)**

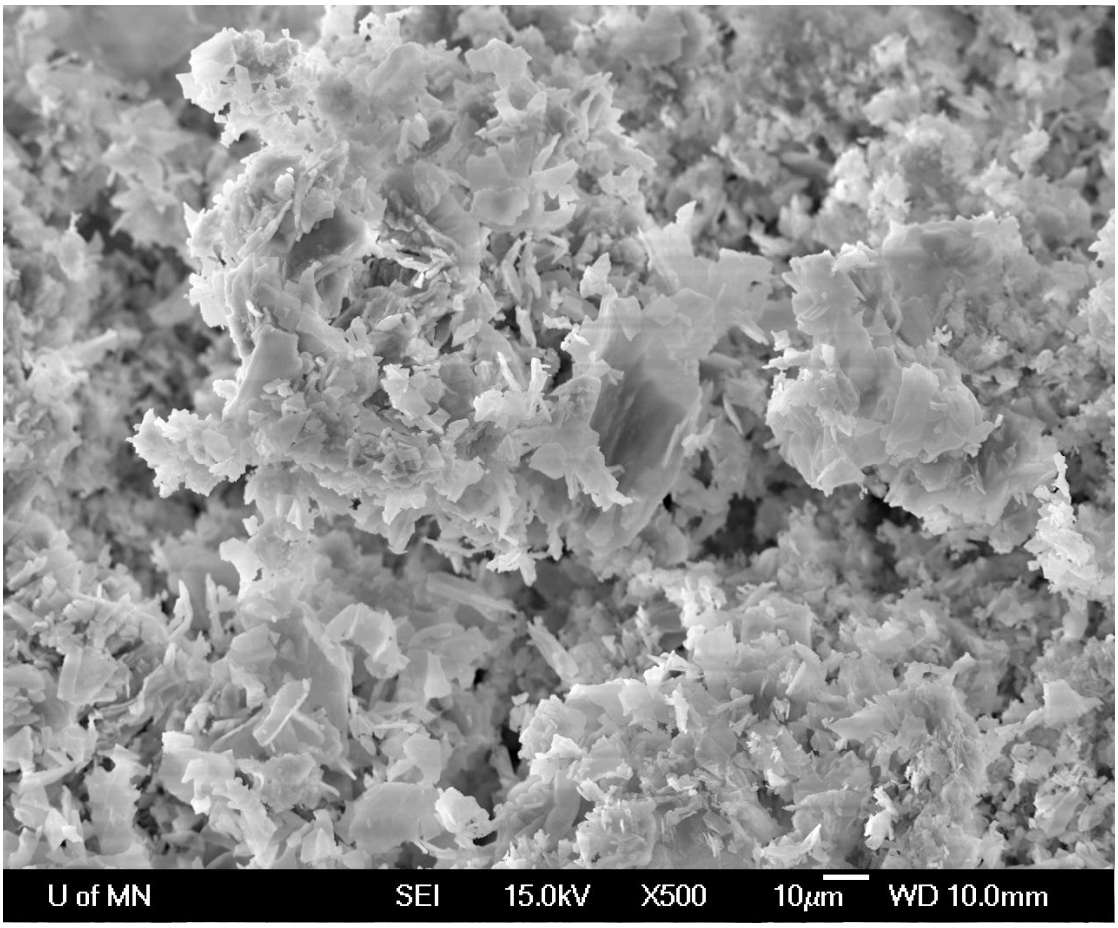


**Figure 30: SEM of Calcium hydroxyapatite pellets**

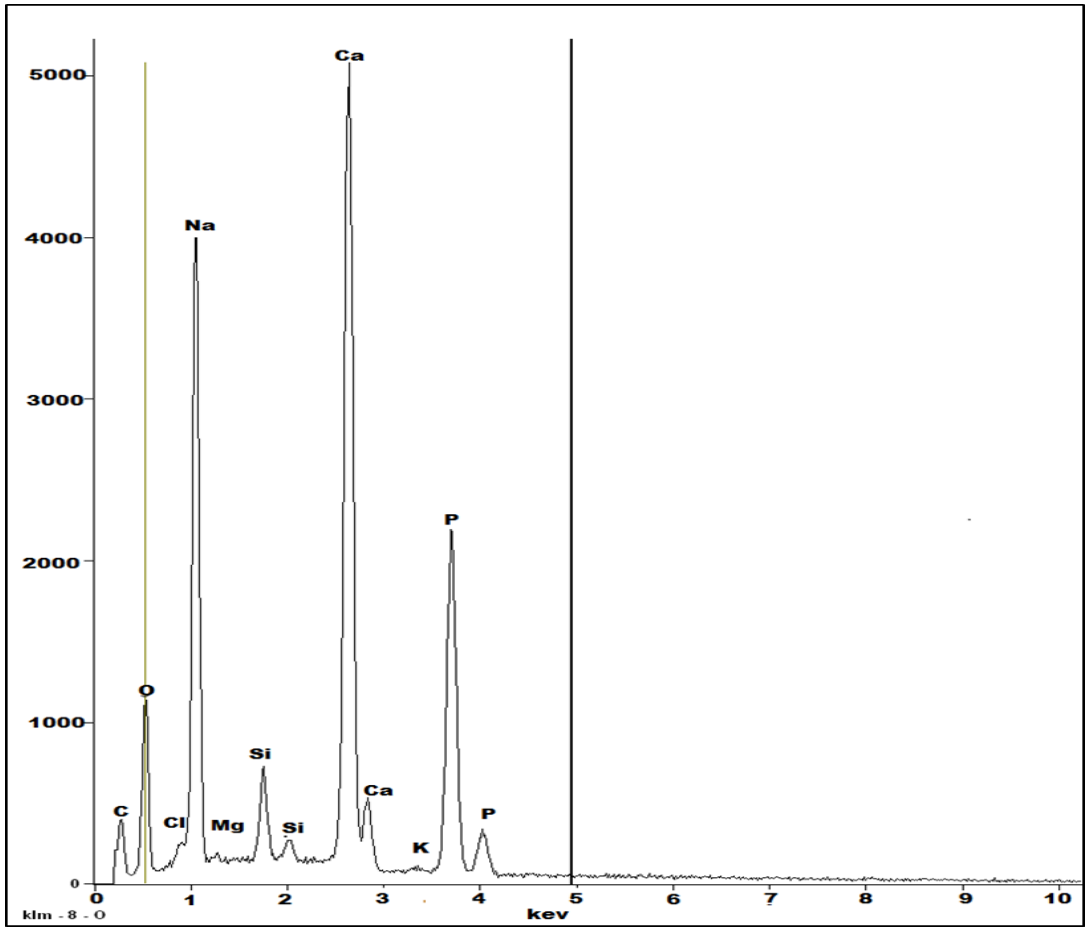


| Element | Percentage (wt.%) |
|---|---|
| Ca | 27 |
| P | 16.9 |

**Figure 31: Chemical analysis of hydroxyapatite crystals**

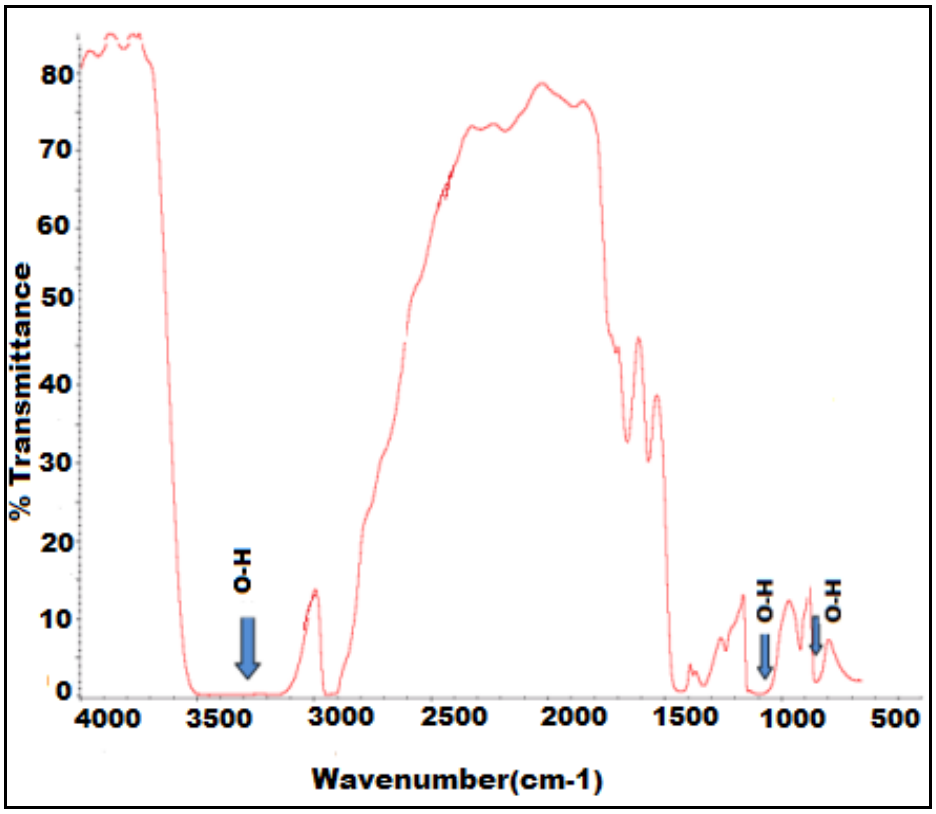


**Figure 32: ATR of Polyvinyl Alcohol**

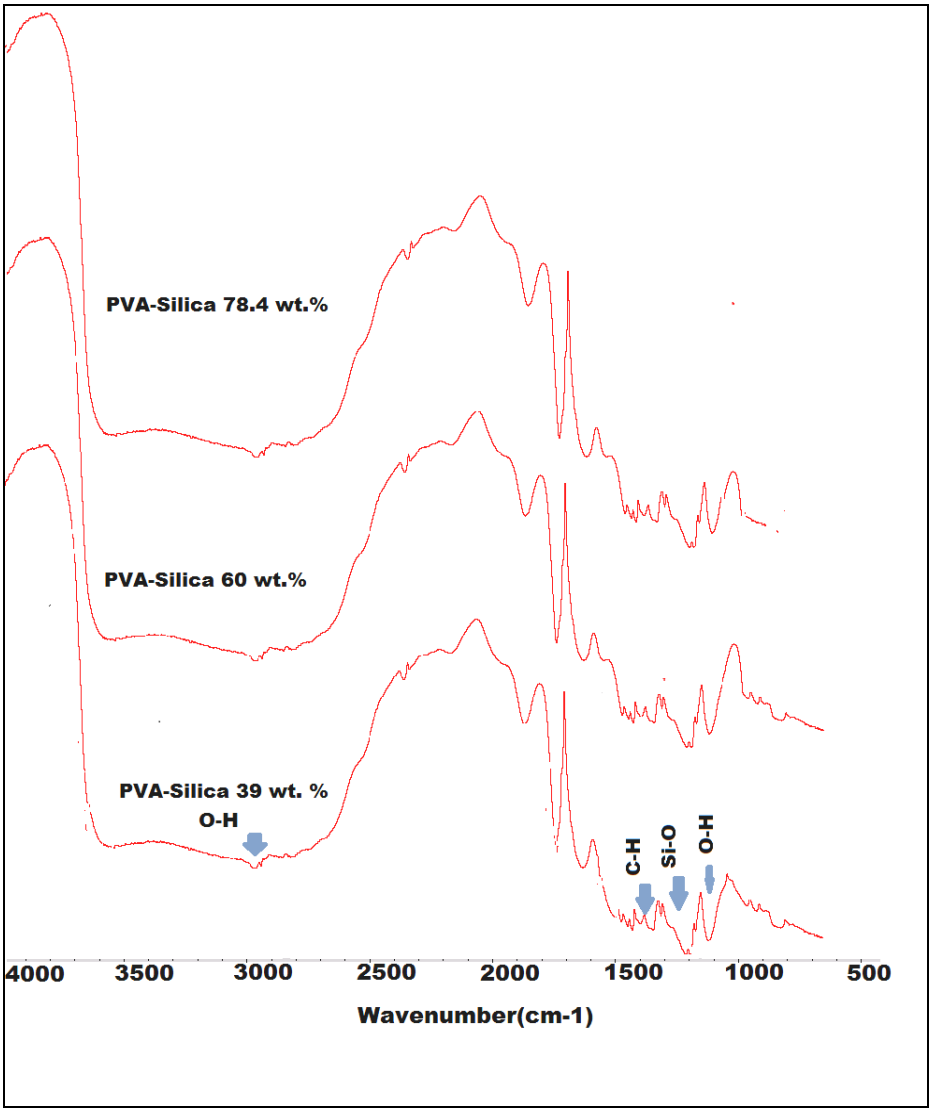


**Figure 33: ATR of Polyvinyl Alcohol-Silica nanocomposite**

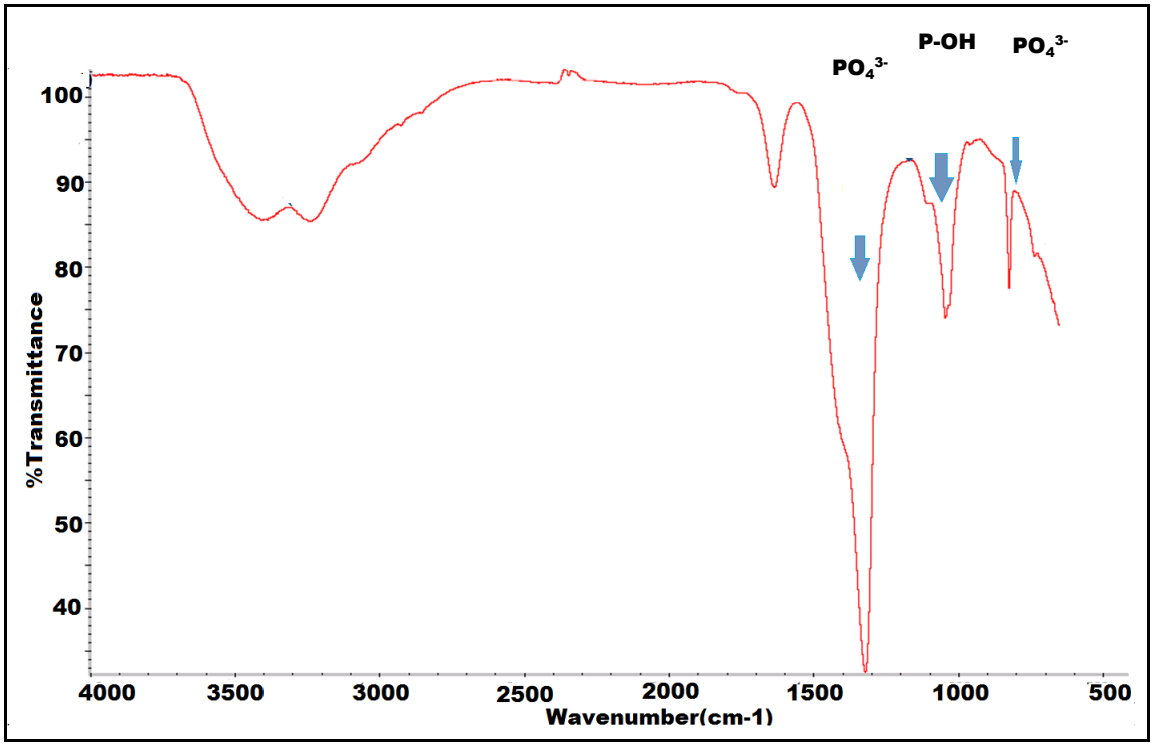


**Figure 34: ATR of calcium hydroxyapatite coated nanocomposite (silica 120 wt. %)**

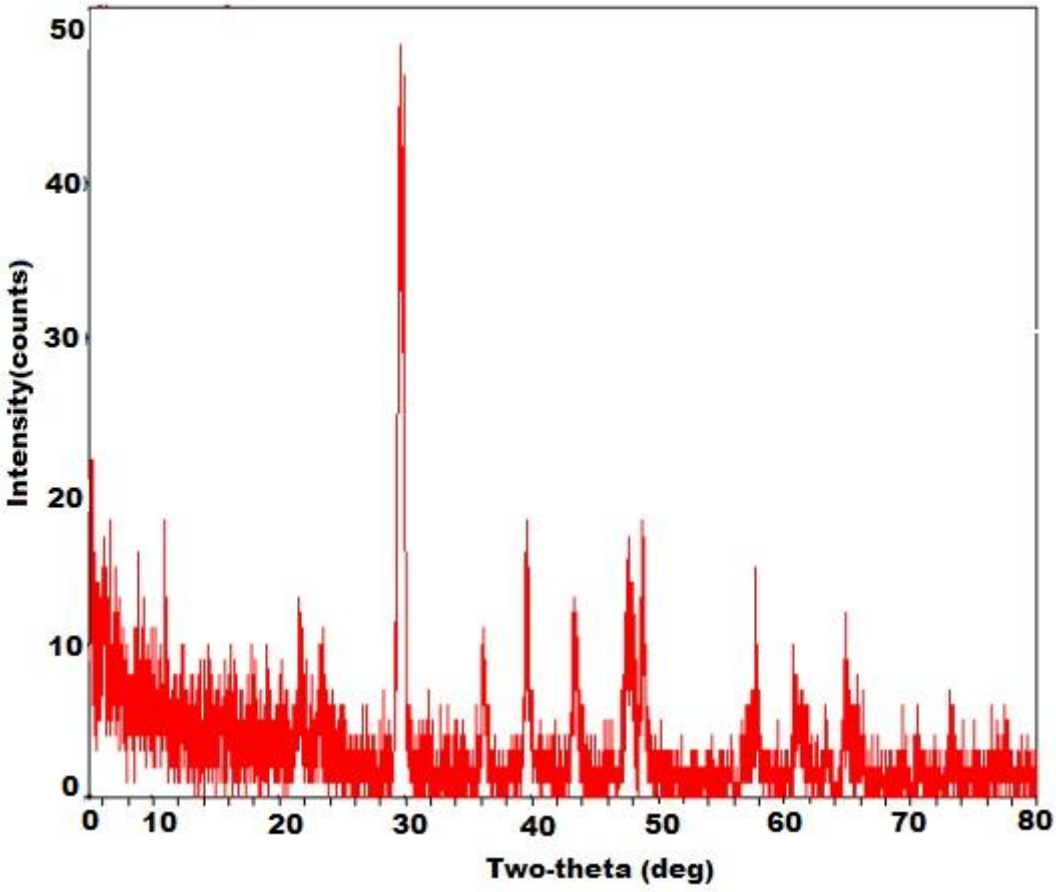


**Figure 35: XRD pattern of Polyvinyl alcohol**

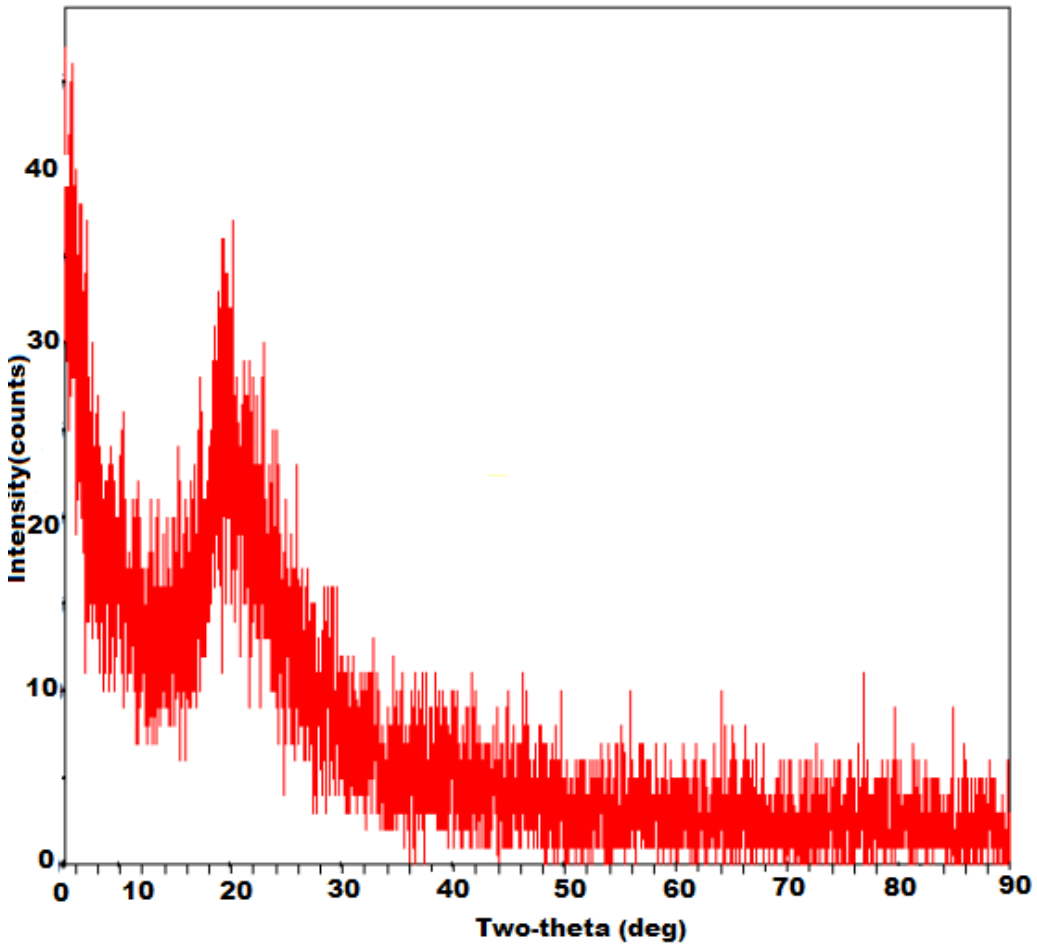


**Figure 36: XRD pattern of nanocomposite (silica 39 wt.%)**

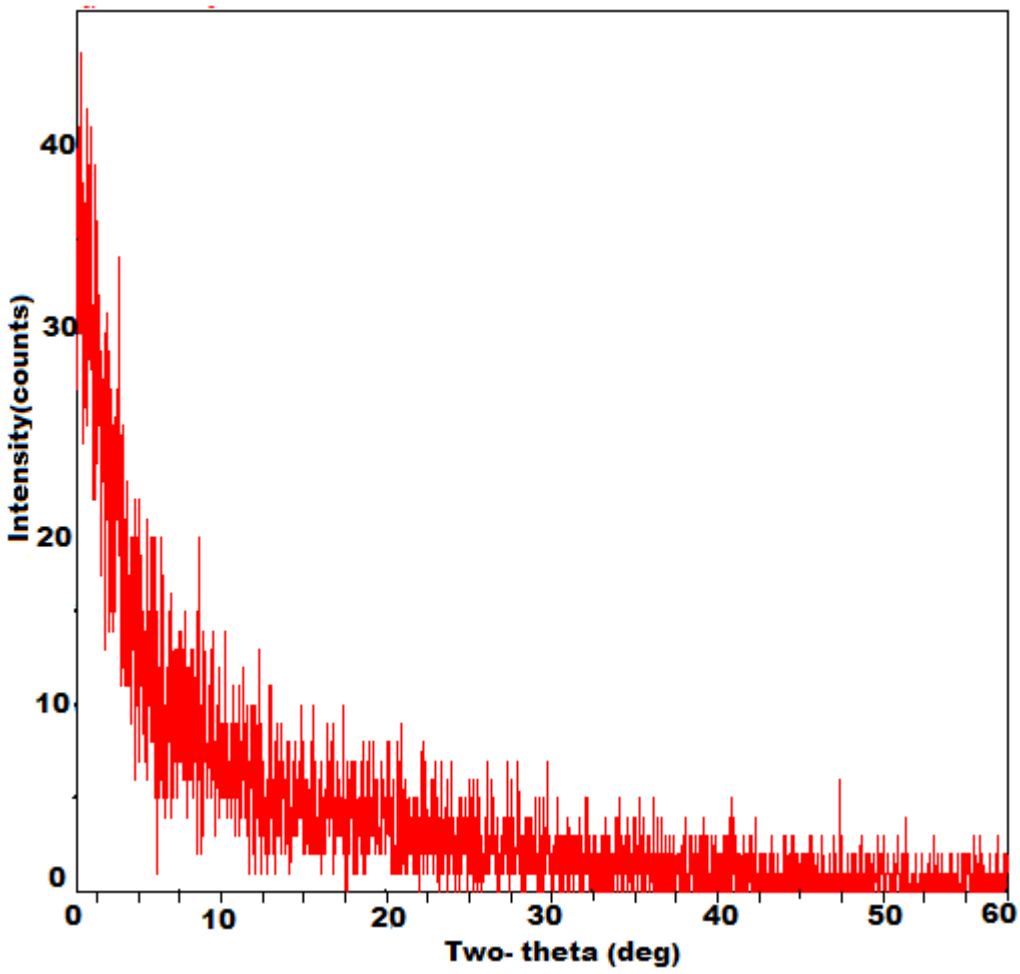


**Figure 37: XRD pattern of nanocomposite (silica 120 wt.%)**

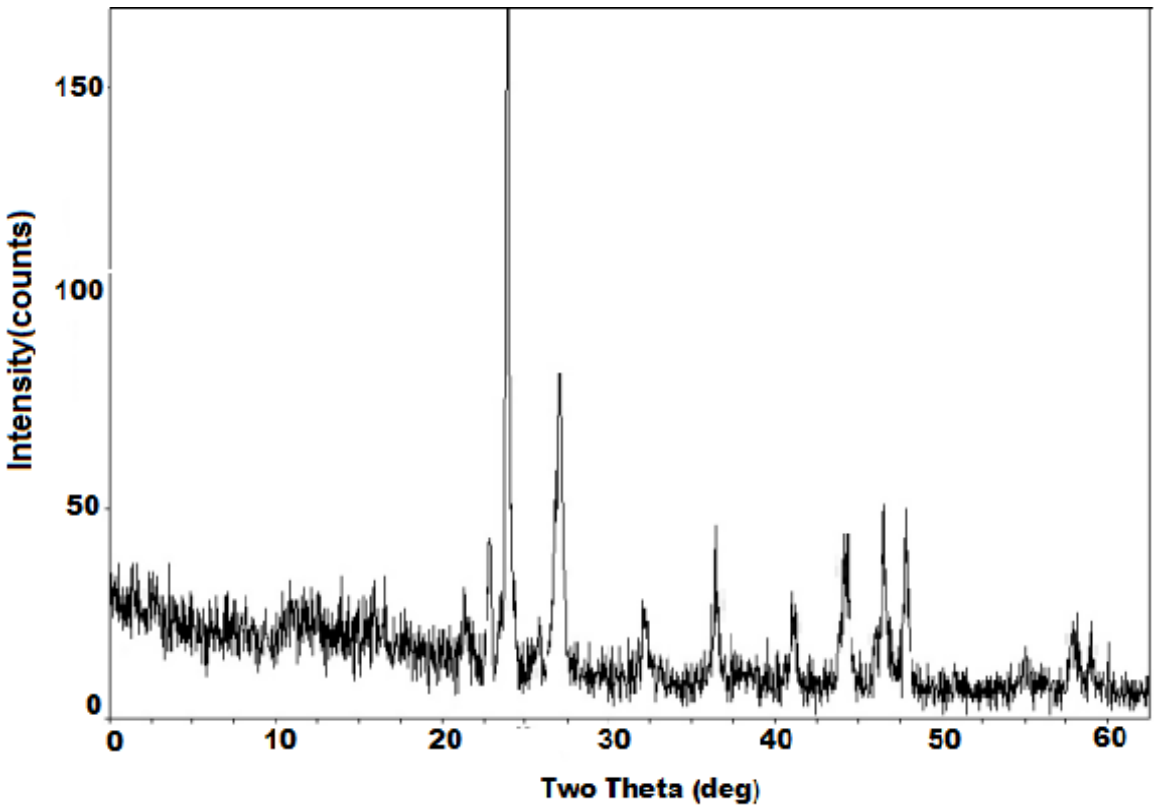


**Figure 38: XRD pattern of calcium hydroxyapatite nanocomposite(silica 120 wt.%)**

## APPENDIX - A

**Acronyms**

Ca HAp- Calcium hydroxyapatite

CNT- Carbon nanotubes

DW-Distilled water

E- Young's Modulus

GPa- Gigapascal

HCl- Hydrochloric acid

LBL- Layer by Layer

MMT- Montmorillonite

PAH- Polyallylamine

PDDA- Polydiallyldimethylammonium

PEO- Polyethylene oxide

PMMA- Polymethmethylacrylate

PP – Polypropylene

PS-Polystyrene

PU-Poly urethane

PVA-Polyvinyl alcohol

RSA – Rheometric Solid Analyzer

SBF- Simulating body fluid

SDS – Sodium dodecyl sulphate

SEM –Scanning electron microscopy

SWCNT- Single wall nanotubes

XRD – X-Ray Diffraction

## APPENDIX - B

### Halpin Tsai Equation

*Modulus calculated for 39 wt. % silica*

Density of silica = 2.2 gm/$cm^3$

Volume of Silica dispersion used= 5.5 ml

Weight of Silica in 5.5 ml of Dispersion = 0.56 gm

Therefore, volume of silica actually present in nanocomposite = (0.56/2.2) = 0.245$cm^3$

Volume of PVA solution used = 14.5 ml

Density of Polyvinyl alcohol = 1.3 gm/$cm^3$

Weight of PVA in solution = 1.45 gm

Therefore, volume of polyvinyl alcohol actually present in nanocomposite = (1.45/1.3) =1.11 $cm^3$

Volume fraction of Silica in nanocomposite = 0.254

Volume fraction of PVA in nanocomposite = 0.813

Ι] = [(198/ 0.3) -1]/ [(198/0.3) +2] =0.99 [Using equation 1]

$E_o$ = 0.3[(1+ 2*0.99*0.81)/ (1-0.99*0.81)] [Using equation 2]

$E_o$ = 4GPa.

**Calculation for Apatite Modulus**

$E_{total} = E_{composite} *(V_{composite}/V_{total}) + E_{apatite}*(V_{apatite}/V_{total})$

$= E_{composite}*(Ax_{composite}/A(x_{composite+}x_{apatite}))+E_{apatite}*(Ax_{apatite}/A(x_{composite+}x_{apatite}))$

$E_{total} = 8(0.04/0.042) + 110(.002/.042)$

$E_{total} = 7.6+5.2$

$E_{total} = 12.8GPa$

$E_{total}$ - Modulus of nanocomposite coated with apatite

$E_{composite-}$ Modulus of nanocomposite

$E_{apatite-}$ Modulus of apatite

$x_{composite}$- thickness of composite film

$x_{apatite}$- thickness of apatite film

A- Area of nanocomposite film

Theoretical modulus of apatite coated nanocomposite is 12.8GPa while the experimental results show a modulus of approx. 11GPa.

**Calculation for Nanoindentation**

*Modulus calculated for 60 wt. % silica*

$$h_p = h_{max} - \varepsilon \frac{P_{max}}{S}$$ [Using equation 3]

Substituting the values from the loading-unloading curve

$h_p = 10^{-9} * (2200) - 0.75 (25*10^{-3}/6.5*10^{4})$

$h_p = 18.9*10^{-7}$m

Substituting the value obtained in equation

$A = 24.56 *369*10^{-14}$ [Using equation 4]

$A = 9054 *10^{-14}$ $m^2$

Calculating modulus using equation 5 for 60 wt. % silica

$$E^* = \left(\frac{1-\upsilon_s^{\,2}}{E_s} + \frac{1-\upsilon_i^{\,2}}{E_i}\right)^{-1}$$

$E = (1/1.096) *(6.5*10^{4}) *(0.5) *\text{sqrt}\ (3.14/9054) *10^{7}$

E = 5.5 GPa

Experimentally obtained modulus = 4.8 GPa

**Calculation of Hardness**

*Hardness calculated for 39 wt. % silica*

$$h_p = h_{max} - \varepsilon \frac{P_{max}}{S}$$ [Using Equation 3]

S= (12.5-5/2200-2000)*1000

S=37500

$h_{max}$= 2200nm, ε= 0.75

$P_{max}$= 12.5mN

Using Equation 3, calculate:

$h_c$= 1.96um

$$H(c) = \frac{P_{max}}{c\, h_c^2}$$

Hardness using the above equation can be calculated.

H = $13.4*10^8$ $N/m^2$